Current Research in Structural Biology 5 (2023) 100101

Contents lists available at ScienceDirect

Current Research in Structural Biology

journal homepage: www.journals.elsevier.com/current-research-in-structural-biology

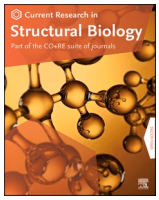

Research Article

Soluble domains of cytochrome *c*-556 and Rieske iron–sulfur protein from *Chlorobaculum tepidu*m: Crystal structures and interaction analysis

Hiraku Kishimoto [a], Chihiro Azai [b], Tomoya Yamamoto [a], Risa Mutoh [c,1], Tetsuko Nakaniwa [c,2], Hideaki Tanaka [c], Yohei Miyanoiri [c,**], Genji Kurisu [c,***], Hirozo Oh-oka [a,d,*]

[a] Department of Biological Sciences, Graduate School of Science, Osaka University, Toyonaka, Osaka, 560-0043, Japan
[b] Graduate School of Life Sciences, Ritsumeikan University, Kusatsu, Shiga, 525-8577, Japan
[c] Institute for Protein Research, Osaka University, Suita, Osaka, 565-0871, Japan
[d] Center for Education in Liberal Arts and Sciences, Osaka University, Toyonaka, Osaka, 560-0043, Japan

ARTICLE INFO

Handling Editor: Dr A Wlodawer

Keywords:
Electron transfer
Green sulfur bacteria
menaquinol:cytochrome *c* oxidoreductase
Reaction center
Rieske/cyt*b* complex

ABSTRACT

In photosynthetic green sulfur bacteria, the electron transfer reaction from menaquinol:cytochrome *c* oxidoreductase to the P840 reaction center (RC) complex occurs directly without any involvement of soluble electron carrier protein(s). X-ray crystallography has determined the three-dimensional structures of the soluble domains of the *CT0073* gene product and Rieske iron-sulfur protein (ISP). The former is a mono-heme cytochrome *c* with an α-absorption peak at 556 nm. The overall fold of the soluble domain of cytochrome *c*-556 (designated as cyt *c*-556$_{sol}$) consists of four α-helices and is very similar to that of water-soluble cyt *c*-554 that independently functions as an electron donor to the P840 RC complex. However, the latter's remarkably long and flexible loop between the α3 and α4 helices seems to make it impossible to be a substitute for the former. The structure of the soluble domain of the Rieske ISP (Rieske$_{sol}$ protein) shows a typical β-sheets-dominated fold with a small cluster-binding and a large subdomain. The architecture of the Rieske$_{sol}$ protein is bilobal and belongs to those of b_6f-type Rieske ISPs. Nuclear magnetic resonance (NMR) measurements revealed weak non-polar but specific interaction sites on Rieske$_{sol}$ protein when mixed with cyt *c*-556$_{sol}$. Therefore, menaquinol:cytochrome *c* oxidoreductase in green sulfur bacteria features a Rieske/cyt*b* complex tightly associated with membrane-anchored cyt *c*-556.

1. Introduction

Cytochrome (cyt) *bc* complexes are multi-subunit membrane-bound enzymes that play central roles in respiratory and photosynthetic electron transport chains functioning in the energy transducing systems of many organisms, including bacteria, archaea, eukaryotic mitochondria, and chloroplasts (Majumder and Blankenship, 2016). They consist of at least three catalytic subunits: Rieske iron-sulfur protein (ISP) with a [2Fe–2S] cluster, cytochrome *b* with two *b*-type (one low potential (b_L) and one high potential (b_H)) hemes, and cyt c_1 or *f* with a *c*-type heme. The Q-cycle mechanism is a well-known explanation for the function of cyt *bc* complexes, which catalyze the oxidation of hydroquinone (QH_2) to quinone (Q) at the Q_o-site and transfer the resultant two electrons in a bifurcation manner to opposite sides to each other across the membrane (Cape et al., 2006). One electron moves to the high-potential chain of the [2Fe–2S]-type Rieske iron-sulfur center and the other via the low-potential chain of two *b*-type hemes to the Q_i-site. A stable semiquinone produced at the Q_i-site is then re-reduced again to QH_2,

Abbreviations: cyt, cytochrome; cyt *c*-556$_{sol}$, soluble domain of cyt *c*-556; ESR, electron spin resonance; ISP, iron-sulfur protein; NMR, nuclear magnetic resonance; *pmf*, proton motive force; Q, quinone; QH_2, hydroquinone; RC, reaction center; Rieske$_{sol}$, soluble domain of Rieske ISP; SAD, single anomalous dispersion; SeMet, selenomethionine.

* Corresponding author. Department of Biological Sciences, Graduate School of Science, Osaka University, Toyonaka, Osaka, 560-0043, Japan.
** Corresponding author.
*** Corresponding author.
E-mail addresses: y-miyanoiri@protein.osaka-u.ac.jp (Y. Miyanoiri), gkurisu@protein.osaka-u.ac.jp (G. Kurisu), ohoka@bio.sci.osaka-u.ac.jp (H. Oh-oka).
[1] Present address: Department of Molecular Biology, Faculty of Science, Toho University, Funabashi, Chiba 274–8510, Japan.
[2] Present address: StemRIM Inc., Saito Bio-Incubator 3F 7-7-15, Saito-Asagi, Ibaraki, Osaka 567–0085, Japan.

https://doi.org/10.1016/j.crstbi.2023.100101
Received 30 December 2022; Received in revised form 4 April 2023; Accepted 11 April 2023
Available online 19 April 2023

following a second turnover at the Q_o-site. Consequently, these electron transport reactions are coupled to proton transfer from the electrochemically negative to the positive side across the membrane, contributing to the production of electrochemical proton gradient, or proton motive force (*pmf*), which is essential for a variety of cellular activities such as ATP synthesis (Kramer et al., 2003).

Recent genome-wide analyses have clearly revealed that cyt *bc* and other related complexes, all of which are involved in the aforementioned QH_2 oxidation coupled with the proton pumping, have a pair of *b*-type hemes and a Rieske iron-sulfur center in common as the catalytic core (Schütz et al., 2000; Nitschke et al., 2010). This invariant functional unit is thought to have diverted into different types of Q-cycle driven energy transducing complexes by incorporating structurally variable and evolutionarily non-conserved electron carriers. For example, cyt bc_1 complex found in α-proteobacteria and mitochondria, and b_6f complex found in photosynthetic cyanobacteria and chloroplasts assemble membrane-bound cyt c_1 and *f* to accept electrons from the Rieske center (Schütz et al., 2000). Moreover, di-heme cyt *c* in ε-proteobacteria, which belongs to the cyt c_4 family and is derived from a tandem repeat of two mono-heme class I-type cyts *c*, is integrated into the membrane to form the complex (Mendz et al., 2000). The C-terminal heme-binding motif (CxxCH) in this di-heme cyt *c* has recently been shown to be disrupted, resulting in mono-heme cyt c_1 in α-proteobacteria and the hyperthermophilic bacterium *Aquifex aeolicus* (Baymann et al., 2004). In the case of *Bacillus* cyt *c*, the three membrane-spanning segments, which are equivalent to subunit IV split from cyt *b*, are fused to small mono-heme cyt *c* reminiscent of cyt *c*-551 on the N-terminal side (Sone et al., 1996).

The genes encoding three subunits of the cyt bc_1 complex—*fbcF* for the Rieske ISP, *fbcB* for cyt *b* and *fbcC* for cyt c_1—exist as a single transcriptional unit of the *fbc* operon in α-proteobacteria, including purple bacteria (e.g., *Rhodobacter capsulatus* and *R. sphaeroides*) (Davidson and Daldal, 1987). However, no *petA* gene (equivalent to *fbcC*) has been found either downstream or upstream of the unit housing the *petC* (*fbcF*) and *petB* (*fbcB*) genes in the green sulfur bacterium *Chlorobium limicola* (Chlorobiacea) (Schütz et al., 1994). A Rieske/-cyt*b*-type complex was therefore proposed to function by donating electrons to the P840 photosynthetic reaction center (RC) complex via the mono-heme cyt *c*-551 subunit (cyt c_z or PscC subunit) (Hauska et al., 2001). Contrary to this, spectroscopic data using membranes from *Chlorobaculum tepidum* has strongly indicated that another membrane-associated cyt *c* with an α-absorption peak at 556 nm, designated as cyt *c*-556, was involved in the direct electron transfer reaction between the Rieske ISP and cyt c_z by playing the role of cyt c_1 (Oh-oka et al., 1998). This has been further confirmed using membranes from a deletion mutant of cyt *c*-554 in *C. tepidum*, showing that the flash-induced electron transfer reaction to the RC complex occurred without any involvement of water soluble cyt *c*-554 (Fig. S1) (Tsukatani et al., 2008). Cyt *c*-554 thus functions as an electron donor to the RC complex from the thiosulfate oxidation pathway (Azai et al., 2009). The *CT0073* gene is considered the most probable candidate encoding cyt *c*-556, judging from its location upstream of *CT0075* encoding cyt *c*-554, because both products appeared to be functionally related to each other in that they both donate electrons independently to the P840 RC complex (Azai et al., 2010). However, the subunit composition of the complex involved in QH_2 oxidation coupled with the *pmf* formation across the membrane is still unknown in green sulfur bacteria, despite its pivotal importance from both mechanistic and evolutionary perspectives.

In this study, the C-terminal domains of CT0073 and the Rieske ISP, both of which were expected to bind redox cofactors and be exposed to the periplasmic space, were successfully overexpressed in *Escherichia coli* cells. The resultant proteins, recovered in soluble states, were designated as CT0073$_{sol}$ and Rieske$_{sol}$ proteins, respectively. The biochemical and physicochemical properties of the CT0073$_{sol}$ agreed with the spectroscopy data on cyt *c*-556 obtained using membranes (Oh-oka et al., 1998; Tsukatani et al., 2008). The crystal structures of both CT0073$_{sol}$ (which more appropriately should be referred to as cyt *c*-556$_{sol}$) and the Rieske$_{sol}$ protein were determined to explore their molecular interaction mechanisms, as the Rieske ISP was supposed to transfer electrons from cyt *b* to cyt *c*-556 by swinging its head domain containing a [2Fe–2S] center (Azai et al., 2010; Iwata et al., 1998). The NMR measurements provided concrete evidence for their direct contact and identified interaction sites on the Rieske$_{sol}$ protein when the complex was formed with cyt *c*-556$_{sol}$. A molecular reaction model by which the electron transfer reaction mechanism could be explained from the Rieske/-cyt*b*-type complex to the P840 RC complex via membrane-anchored cyt *c*-556 is presented.

2. Results

2.1. Biochemical analyses of cyt c-556$_{sol}$

Truncated CT0073, which was expressed in the presence of the pEC86 plasmid in *E. coli*, was a soluble protein and held a *c*-type heme with an α absorption peak at 556 nm (Fig. S2A). Therefore, this protein is referred to as cyt *c*-556$_{sol}$ henceforth. The redox titration curve of cyt *c*-556$_{sol}$ was obtained by plotting the peak heights of its α-absorption band against the ambient potentials (E_h) (Fig. S2B). The data points were fitted with a Nernst curve when the presence of one redox component was postulated, indicating that cyt *c*-556$_{sol}$ has a single heme *c* as deduced from its amino acid sequence information. The redox midpoint potential (E_m) of heme was calculated to be +190 mV, which was almost the same as that reported previously for *c*-type cyt responsible for the electron transfer reaction between the Rieske ISP and cyt c_z (Oh-oka et al., 1998; Okumura et al., 1994; Oh-oka et al., 1995). Furthermore, the presence of CT0073 was confirmed to be expressed as cyt *c*-556 in chlorosome-depleted membranes by nLC/MS/MS analysis of peptides produced by tryptic digestion of heme-bound proteins (Fig. S3).

Flash-induced absorption changes. We previously demonstrated an electron transfer scheme from the Rieske center to the P840, as follows (Oh-oka et al., 1998).

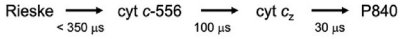

The E_m values of P840, cyt c_z and the Rieske center were reported to be +230 to +240, +170 to +180 mV (or +188 mV as determined as an isolated protein), and +130 to +150 mV, respectively (Okumura et al., 1994; Kjær and Scheller, 1996; Hirano et al., 2010; Knaff and Malkin, 1976). That of cyt *c*-556 was presently determined to be +190 mV (see Fig. S2B). After the photo-oxidized $P840^+$ was re-reduced by a primary electron donor, cyt c_z, with a half time of 30 μs ($t_{1/2}$ = 30 μs), the oxidized cyt c_z was partially re-reduced by cyt *c*-556 with $t_{1/2}$ = 100 μs due to a small difference of their redox potentials. The oxidized states of cyts c_z and *c*-556 were then kept during several milliseconds, suggesting that they formed a relatively stable complex (Oh-oka et al., 1998).

The above electron transfer reactions regarding to cyts *c* were tracked again by flash photolysis (Figs. S4A and B). In the present time resolution of a millisecond, rapid absorption decreases were detected at 552 and 556 nm immediately after flash excitation, indicating that the equilibration between hemes c_z and *c*-556 was attained within 1 ms as expected from the previous measurements (Oh-oka et al., 1998). Therefore, distribution of the one positive charge between cyts c_z and cyt *c*-556 in the quasi equilibration state was estimated to be approximately 0.45:0.55 by the Nernst equation ($\Delta E_m = RT/F \ln K$). Then, both of them were re-reduced slowly with $t_{1/2}$ = 50–100 ms by ascorbate added to the reaction medium and/or the back reaction from the terminal electron acceptor(s) in the RC, due to the presence of stigmatellin which inhibited the electron transfer reaction from the Rieske center by binding to the Q_o-site (Von Jagow and Link, 1986).

However, after the addition of excess cyt *c*-556$_{sol}$, the absorption intensity at 556 nm showed an additional increase of approximately

20–30% within the first of several milliseconds ($t_{1/2}$ = ~3 ms) (Fig. S4B). This implies that the additional cyt *c*-556$_{sol}$ transferred electrons independently to cyt c_z with $t_{1/2}$ = ~3 ms. In contrast to this, the difference extent at 552 nm observed in a few milliseconds was almost unchanged, indicating that a part of cyts c_z still remained in the oxidized state when difference absorption spectra of cyt c_z and cyt *c*-556 were compared to each other (see Fig. S4C). These findings suggested that the equilibration among three hemes—heme c_z in cyt c_z, heme *c*-556 in the intrinsic membrane-bound cyt *c*-556 (designated as cyt *c*-556$_{intr}$), and heme *c*-556 in the exogenously added cyt *c*-556$_{sol}$—was attained within this time range. As demonstrated in the *in vitro* reconstitution experiments using water-soluble cyt *c*-555, the C-terminal domain of cyt c_z could take two different orientations during a series of reaction processes; two complex states of cyt *c*-556$_{intr}$/cyt c_z and cyt *c*-555/cyt c_z were supposed to be in equilibrium with each other (Tsukatani et al., 2008). In a similar way, relatively stable states of cyt *c*-556$_{intr}$/cyt c_z and cyt *c*-556$_{sol}$/cyt c_z appeared to be formed (see Fig. S4D). Thus, the relative amounts of oxidized heme c_z and heme *c*-556 (cyt *c*-556$_{intr}$ and cyt *c*-556$_{sol}$) were roughly estimated to be 0.30–0.35 and 0.70–0.65, respectively, from their difference extents at 552 and 556 nm, respectively.

In the present study, the electron-transfer rate from cyt *c*-556$_{sol}$ to cyt c_z in the membranes yielded a $t_{1/2}$ = ~3 ms in the presence of an excess amount of cyt *c*-556$_{sol}$. It is therefore rational to consider that its second-order rate constant would be approximately the same value as that (1.7×10^7 M^{-1} s^{-1}) reported for soluble cyt *c*-554 which donates electrons to cyt c_z, because the latter electron-transfer rate was almost the same ($t_{1/2}$ = ~3 ms) when measured under similar experimental conditions (Tsukatani et al., 2008; Itoh et al., 2002).

2.2. Structural characterization of cyt *c*-556$_{sol}$

Crystallization and structure determination of cyt c-556$_{sol}$. Cyt *c*-556$_{sol}$ protein obtained after gel filtration chromatography was confirmed to have sufficient purity for crystallization (Fig. S5A). Crystals of cyt *c*-556$_{sol}$ were obtained by hanging-drop vapor diffusion method at 293K. A hanging drop was prepared by mixing equal volumes of protein solution and reservoir solution containing 0.1 M sodium acetate trihydrate (pH4.4) and 1.8M ammonium sulfate. The sizes of small crystals were approximately 0.3 mm × 0.3 mm x 0.3 mm (Fig. S5B). For cryoprotection, the crystals were transferred to a solution containing 0.1M sodium acetate (pH4.6), 2.0M ammonium sulfate, and 20% (v/v) glycerol. Data for iron (Fe) single anomalous dispersion (SAD) phasing were collected at 100K on the SPring-8 beamline BL44XU (Harima, Hyogo, Japan). The crystals diffracted X-rays at a maximum resolution of 1.65 Å resolution (Fig. S5C). The crystals belong to space group $P6_422$ with unit-cell parameters a = 85.02 Å, b = 85.02 Å, c = 123.93 Å, α = β = 90°, and γ = 120°. The diffraction data were processed and scaled using the program HKL-2000 (Otwinowski and Minor, 1997). The initial phase was determined by Fe-SAD method with the program AutoSol in PHENIX program suite at 1.65 Å resolution (Fig. S5D) (Liebschner et al., 2019; Terwilliger et al., 2009). Cyt *c*-556$_{sol}$ had single iron atom in heme *c*. The initial electron density map revealed most of the main chains and side chains. Molecule and asymmetric unit contained two molecules of cyt *c*-556$_{sol}$. The structure model was manually built using the program COOT in CCP4 (Emsley and Cowtan, 2004), and refined using REFMAC5 in CCP4 and PHENIX refine (Liebschner et al., 2019; Winn et al., 2011; Murshudov et al., 1997). The statistics for the data collection and refinement are given in Table 1.

Overall structure of cyt c-556$_{sol}$. Cyt *c*-556$_{sol}$ was expressed as the water-soluble C-terminal heme-containing moiety of membrane-anchored cyt *c*-556, and crystallized as a globular molecule with dimensions of approximately 30 × 30 × 30 Å (Fig. S5). The scaffold of the molecule was formed by four α-helices holding the heme prosthetic group without any β-sheets (Fig. 1A). Its overall structure followed the topology of typical class I *c*-type cyts (Ambler, 1991). According to the criteria proposed by Kabsch and Sander (1983), Gly72 divides the N-terminal helix into two parts. The polypeptide thus consists of α1 (residues 66–71), α1' (residues 75–79), α2 (residues 92–100), α3 (residues 103–112), and α4 (residues 128–140) helices. The iron ion of heme *c* is coordinated to His79Nε2 of the α1′ helix and Met117S of the loop region between the α3 and α4 helices as the fifth and sixth ligands, respectively (Fig. 1B). In addition, two vinyl groups of heme *c* are covalently bonded to Cys75Sγ and Cys78Sγ of the α1' helix. The heme prosthetic group is almost entirely buried within a hydrophobic crevice, leaving only a slight edge of the heme ring II and the propionate side-chain of ring III exposed to solvent. These structural features of cyt *c*-556$_{sol}$ are similar to those of other class I *c*-type cyts as mentioned below.

Table 1
Crystallographic data and refinement statistics.

	cyt *c*-556$_{sol}$		Rieske$_{sol}$ protein
	native	SAD	SAD
Crystallographic data			
X-ray source	SPring-8 BL44XU	SPring-8 BL44XU	SPring-8 BL44XU
Wavelength (Å)	0.90000	1.70000	0.97919
space group	$P6_422$	$P6_422$	$C2$
Unit cell parameters			
a (Å)	85.02	85.02	130.64
b (Å)	85.02	85.02	58.70
c (Å)	123.93	123.93	49.68
α (deg)	90	90	90
β (deg)	90	90	112.04
γ (deg)	120	120	90
Resolution range (Å)	50.00–1.65 (1.68–1.65)[a]	50.00–1.90 (1.93–1.90)[a]	60.55–2.13 (2.24–2.13)[a]
Total no. reflections	675134	435345	74670
No. of unique reflections	32195 (3113)	21625 (1045)	15654 (1581)
Completeness (%)	99.9 (100)[a]	100 (100)[a]	99.8 (99.0)[a]
R_{merge} (I) (%)[b]	0.056 (0.240)[a]	0.092 (0.503)[a]	0.112 (0.604)[a]
I/σ	95.6 (23)[a]	47.1 (4.8)[a]	8.9 (2.7)[a]
Redundancy	20.7 (21.2)[a]	20.2 (19.5)[a]	7.4 (7.1)[a]
Refinement statistics			
Resolution range (Å)	36.82–1.65 (1.71–1.65)	–	60.55–2.30 (2.36–2.30)
Reflections used in refinement	32194 (3113)	–	15648 (1580)
R_{work}[c]	0.153	–	0.200
R_{free}[d]	0.173	–	0.241
Mean B value (Å^2)	20.115	–	55.524
No. of non-hydrogen atoms			
protein	1130	–	1634
heme/metal cluster/ion	106	–	34
water	192	–	78
RMSD from ideal values			
bond length (Å)	0.033	–	0.021
bond angles (deg)	3.306	–	2.233

[a] Values in parentheses are for the highest resolution shells.
[b] R_{merge} $(I) = \Sigma|I(k) - \langle I\rangle|/\Sigma I(k)$ representing the k value of an intensity measurement of a reflection, $\langle I\rangle$ the mean intensity value of that reflection, and Σ the summation across all measurements.
[c] R-factor $= \Sigma||F_{obs}(hkl)| - |F_{calc}(hkl)||/\Sigma|F_{obs}(hkl)|$.
[d] R_{free} is the R-factor computed for the test set of reflections that were omitted from the refinement process.

Structural similarities to other cytochromes c. The overall structural comparisons of the presently determined *C. tepidum* cyt *c*-556$_{sol}$ using the Dali server (Holm, 2022) revealed extensive similarities to those of cyt c_5 from the nitrogen-fixing soil bacterium *Azotobactor vinelandii* (PDBID 1CC5, Z-score of 11.9) (Carter et al., 1985), cyt *c*-551 from the halophilic purple photosynthetic bacterium *Halorhodospira halophila* (PDBID 1GKS, Z-score of 11.5) (Bersch et al., 1996), cyt c_6 from the cyanobacterium *Phormidium laminosum* (PDBID 2V08, Z-score of 9.7) (Worrall et al., 2007), and cyt *c*-554 from the green sulfur bacterium *C. tepidum* (PDBID 4J20, Z-score of 15.5) (see Fig. 2) (Yu et al., 2013). All

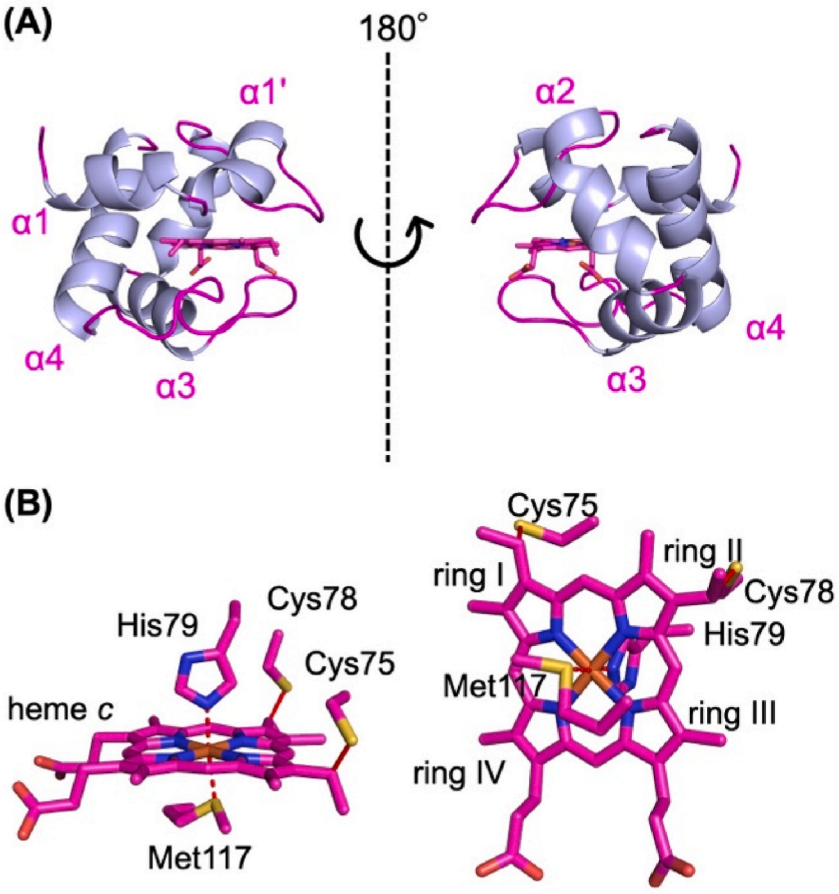

Fig. 1. Structure of cyt *c*-556$_{sol}$. (A) Ribbon representation of cyt *c*-556$_{sol}$. The α -helices are shown in light blue. (B) Close-up views of heme *c* from the horizontal (left) and the sixth ligand sides (right). Coordinate bonds between heme *c* and ligands are shown as red dotted lines and thioether bonds red solid lines. These figures were created with PyMOL (The PyMOL Molecular Graphics System, Version 2.0). (For interpretation of the references to color in this figure legend, the reader is referred to the Web version of this article.)

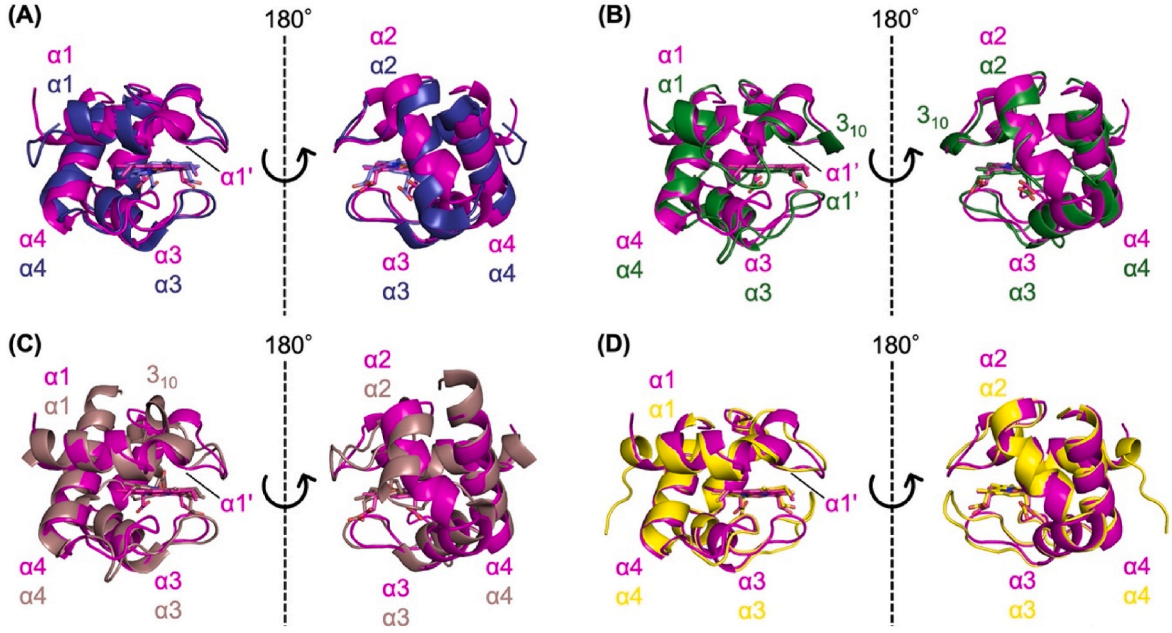

Fig. 2. Structure comparison of the *C. tepidum* cyt *c*-556 (magenta) with (A) cyt c_5 from *Azotobactor vinelandii* (dark blue; PDBID 1CC5), (B) cyt *c*-551 from *Halorhodospira halophila* (dark green; PDBID 1GKS), (C) cyt c_6 from *Phormidium laminosum* (light blown; PDBID 2V08) and (D) cyt *c*-554 from *C. tepidum* (yellow; PDBID 4J20) by superposition of their polypeptide chains with PyMOL. (For interpretation of the references to color in this figure legend, the reader is referred to the Web version of this article.)

these cyts *c* contained four α-helices in common without any β-sheets, as expected from the structural characteristics of class I *c*-type cyts, although the N-terminal helix, α1′, was missing in the case of cyt c_5. The loop structures also seemed to be slightly different among them; the loop between α1 and α1' in cyt *c*-551 was longer than others, and the loops between α3 and α4 in both cyt *c*-551 and cyt c_6 were bent and protruding in different directions. The additional 3_{10}-helices were found between α2 and α3 in both cyt *c*-551 and cyt c_6, but each of them was in a spatially different location.

Root-mean-square deviation (RMSD) values were also calculated by using pairwise structure comparison on the Dali server to estimate the degree of structural deviation from each other (Holm, 2022). Interestingly, the structure of *C. tepidum* cyt *c*-556$_{sol}$ exhibited the highest similarity to cyt *c*-554 with an RMSD value of 1.0. In both cytochromes, the heme groups are exposed to their surfaces at the sides of pyrrole rings II and III. However, the longer loop connecting the α3 and α4 helices in cyt *c*-554, compared to that in cyt *c*-556, covers most of the pyrrole ring III, leaving only the oxygen atom of propionate exposed to the solvent. Because both cyts *c* donate electrons directly to the P840 in the photosynthetic RC independently (Oh-oka et al., 1998; Tsukatani et al., 2008; Itoh et al., 2002), the different protein surface natures around the heme-exposed edges between them might be involved in the reaction specificity to the P840, as mentioned below.

Surface properties. Most of the protein surface area of cyt *c*-556 was covered with charged and polar residues (Fig. 3), and the heme group was largely embedded in the hydrophobic interior. The only parts that are solvent-accessible in heme are the edges at the sides of the pyrrole rings II and III. The protein surface around the pyrrole ring II edge consists of several non-polar residues and is relatively hydrophobic, as seen in cyt *c*-554. The hydrophobic patch is considered an electron transfer gate, and the hydrophilic area around the patch is responsible for complex formation, as reported in detail for water-soluble cyt c_6 functioning as an electron donor in photosystem I and cyt c_2 in the RC of purple bacteria (Tetreault et al., 2002; Sommer et al., 2006).

Conversely, the protein surface around the pyrrole ring III edge is a less positively charged and rather non-polar area, compared to that in cyt *c*-554, especially in the portion flanking the pyrrole ring II (also see Fig. S6). As discussed later, this non-polar region is important for the formation of the electron transfer complex with the Rieske ISP, as determined from the NMR experimental data demonstrated in the following section. Two positively charged residues (lysine [Lys]56 and Lys59) in cyt *c*-554, one (Lys56) of which resides in a unique long loop between the α3 and α4 helices, would therefore be involved in its specific interaction with cyt c_z of the P840 RC complex. Cyt *c*-554 has been demonstrated to donate electrons to cyt c_z via the sulfur-oxidation pathway and not to mediate the electron transfer reaction between the Rieske/cyt*b* complex and the P840 RC complex (Tsukatani et al., 2008).

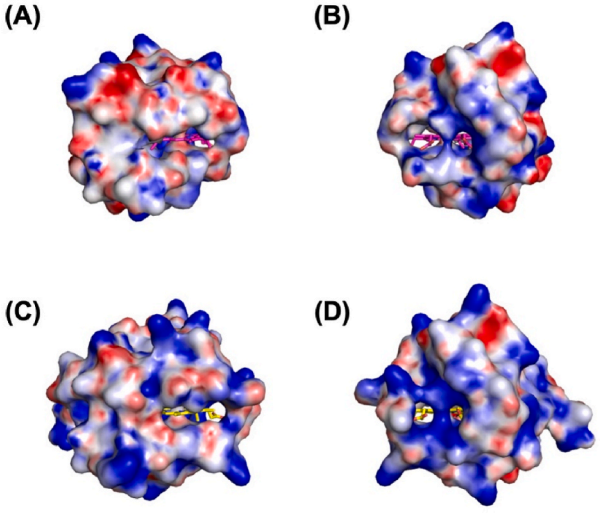

Fig. 3. Electrostatic properties of the surfaces of cyts *c*-556$_{sol}$ and *c*-554. The distribution is colored according to the electrostatic potential from $-10K_BT$ (red) to $+10$ K_BT (blue) calculated with PyMOL APBS (the Adaptive Poisson-Boltzmann Solver) Tools (Baker et al., 2001; Dolinsky et al., 2004). (A) and (B) represent the surfaces of the vinyl- and propionate-group sides, respectively, of heme *c* (shown in magenta) in cyt *c*-556. (C) and (D) represent those of heme *c* (shown in yellow) in cyt *c*-554 in the same way. (For interpretation of the references to color in this figure legend, the reader is referred to the Web version of this article.)

2.3. Structural characterization of selenomethionine (SeMet)-Rieske$_{sol}$ protein

Crystallization and structure determination of SeMet-Rieske$_{sol}$ protein. The SeMet-Rieske$_{sol}$ protein obtained after Ni^{2+}-*NTA* affinity column and subsequent gel filtration chromatography was confirmed to have sufficient purity for crystallization (Fig. S7A). Crystals of SeMet-Rieske$_{sol}$ protein were obtained by hanging-drop vapor diffusion method at 293 K. A hanging drop was prepared by mixing equal volumes of protein solution and reservoir solution containing 0.1 M ammonium citrate (pH 5.0), 0.2 M ammonium sulfate, 22% (w/v) polyethylene glycol 2,000 and 10% (v/v) ethanol. The crystal showed a truncated square pyramid shape with clear edges. The sizes were approximately 0.1 mm × 0.2 mm × 0.1 mm (Fig. S7B). For cryoprotection, the crystals were transferred to a solution containing the same buffer as crystallization buffer with 20% (v/v) ethanol. Data for selenium (Se)-SAD phasing were collected at 100K on the SPring-8 beamline BL44XU. The crystals diffracted X-rays at a maximum resolution of 2.1 Å (Fig. S7C). The crystals belong to space group *C*2 with unit-cell parameters a = 130.8 Å, b = 58.7 Å, c = 49.8 Å, α = γ = 90°, and β = 112.1°. The diffraction data were processed and scaled using the program HKL-2000 (Otwinowski and Minor, 1997). The initial phase was determined by Se-SAD method with the program AutoSol in PHENIX program suite at 2.3 Å resolution (Fig. S7D) (Liebschner et al., 2019; Terwilliger et al., 2009). The SeMet derivative protein had single SeMet residue and single site was found. The initial electron density map revealed most of the main chains and side chains. Molecule and asymmetric unit contained two molecules of Rieske$_{sol}$ protein. The structure model was manually built using the program COOT in CCP4 (Emsley and Cowtan, 2004), and refined using REFMAC5 in CCP4 (Winn et al., 2011; Murshudov et al., 1997). The statistics for the data collection and refinement are presented in Table 1.

Overall structure of the Rieske ISP soluble domain. The soluble domain of the Rieske ISP (Rieske$_{sol}$ protein) is a globular elliptical molecular structure with dimensions of approximately 30 × 40 × 40 Å. The scaffold of the molecules was formed using three antiparallel β-sheets. Sheet 1 is formed by β-strands β1 (residues 82–88), β8 (residues 168–172), and β9 (residues 175–181); sheet 2 by β-strands β2 (residues 96–103), β3 (residues 106–113), and β4 (residues 116–121); and sheet 3 by β-strands β5 (residues 132–134), β6 (residues 138–141), and β7 (residues 146–149) (Fig. 4A). The structure does not contain an α-helix in its scaffold, as is usually present in the Rieske ISPs determined to date. However, two 3_{10} helices (residues 90–92 and 135–137) are present between β1 and β2, and β5 and β6 instead.

The structure of the Rieske$_{sol}$ protein can be divided into two subdomains (Bönisch et al., 2002; Veit et al., 2016). One is a small cluster-binding subdomain that contains a [2Fe–2S] cluster constituted on a scaffold β-sheet 3 (β5–β7) along with ligand loops 1 and 2 and the proline loop (described below). The other is a large subdomain that consists of β-sheets 1 (β1, β8, β9) and 2 (β2–β4). Each subdomain appears to constitute an incomplete antiparallel barrel structure, whereas the overall folding motif of β-strands is regarded as a common feature of the Rieske ISPs, as described in detail below.

The cluster-binding site is formed by cluster-binding loops β4–β5 (loop1, residues 122–131) and β6–β7 (loop2, residues 143–145) and the

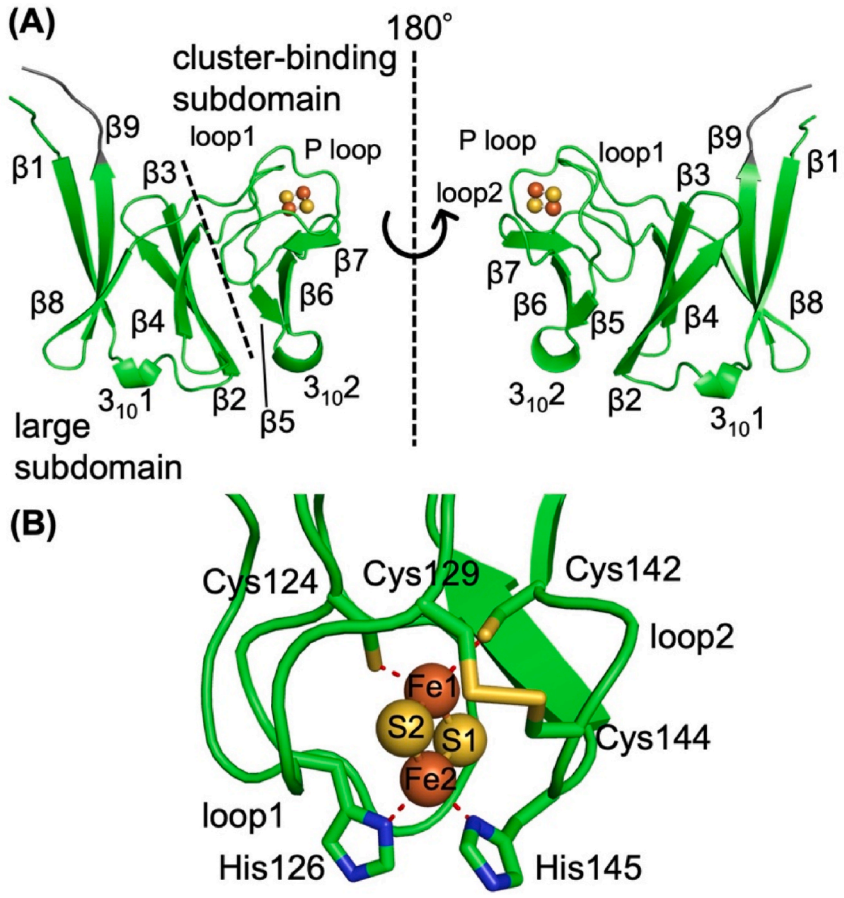

Fig. 4. (A) Structure of the soluble domain of the Rieske ISP (Rieske$_{sol}$ protein) from *C. tepidum*. His-tag region in the C-terminus is colored with grey. It contains nine β-sheets and two 3_{10} helices. (B) Close-up view of the [2Fe–2S] cluster in (A). Bonds between [2Fe–2S] cluster and ligand residues are shown as a red dotted line. Cys129 in loop1 and Cys144 in loop2 form a disulfide bond (shown in yellow) to stabilize the structure around [2Fe–2S] cluster. (For interpretation of the references to color in this figure legend, the reader is referred to the Web version of this article.)

proline loop (P-loop, β8–β9, residues 158–165). Iron ion Fe1 is coordinated by Cys124Sγ from loop1 and Cys142Sγ from loop2, and iron ion Fe2 is ligated by His126Nδ1 from loop1 and His145Nδ1 from loop2 (Fig. 4B). Cluster-binding loops 1 and 2 are stabilized by a disulfide bridge between Cys129 and Cys144. The atomic structure provides direct evidence for the correct insertion of the iron-sulfur cluster into the Rieske$_{sol}$ apoprotein during heterogeneous expression in *E. coli*, as indicated by our previous electron spin resonance (ESR) measurement (Nagashima et al., 2017).

Structure of the [2Fe–2S] cluster. The geometries of the [2Fe–2S] clusters of various Rieske ISPs were compared to determine any differences in their bond lengths and bond angles (Table S1). Although the number of hydrogen bonds was different among these five species, no significant differences were observed in the respective bond lengths and bond angles in the [2Fe–2S] cluster. The only slightly different bond length was found between the iron atom Fe2 and His126Nδ in the Rieske$_{sol}$ protein of *C. tepidum*, which might have been distorted by SeMet displacement at a residue 129.

Structural similarities with other Rieske ISPs. The structure of the Rieske$_{sol}$ protein from *C. tepidum* determined in the present study was compared with that of the soluble domains of the Rieske ISPs from spinach chloroplasts (PDBID 1RFS, RMSD of 2.6) (Carrell et al., 1997), *Mastigocladus laminosus* (PDBID 1VF5, RMSD of 2.9) (Kurisu et al., 2003), bovine heart (PDBID 1RIE, RMSD of 2.9) (Iwata et al., 1996), and *Paracoccus denitrificans* (PDBID 2YIU, RMSD of 5.0) (Kleinschroth et al., 2011) by superimposition with PyMOL (Fig. S8). Their RMSD values were also calculated using the Dali server (Holm, 2022). Ligand loops 1 and 2 and the proline loop in the cluster-binding subdomain were nearly identical, but the folding in the large subdomain seemed to be somewhat dissimilar, as will be mentioned. The structure of the *C. tepidum* Rieske$_{sol}$ protein exhibited the highest similarity to that of the PetC3 protein (PDBID 5CXM, RMSD of 1.9) (Fig. S9) (Veit et al., 2016). The PetC3 protein is believed to be located in a periplasmic fraction and to anchor to the plasma membrane through the fatty acid chain covalently bound to the N-terminal cysteine residue (Veit et al., 2016). Although proteomic analysis of the PetC3-defected strain indicated a disorder in the nitrogen-related metabolic system, the distinct function of this protein has not yet been revealed.

The three-dimensional structures of the Rieske ISP soluble domains demonstrated that the proteins from cytochrome b_6f and bc_1 complexes could be related to each other, when their sequence alignment was constructed based on not only a simple pair-to-pair comparison of the amino acid sequences, but also the similarity of the folding topologies (Fig. S10). The *C. tepidum* Rieske$_{sol}$ protein is a b_6f-type proteins. However, the insertion between β-2 and β-3 was relatively shorter (only two residues) and the C-terminal extension of 14–15 residues was missing. Its architecture was nevertheless bilobal, as indicated for b_6f-type proteins (see Fig. S8) (Carrell et al., 1997). The linker region of only six residues was also relatively shorter than the typical linkers (approximately 13–15 residues) of the b_6f- and bc_1-type proteins. As the linker regions were involved in the flexible movements of soluble domains, this might suggest a close spatial distance between cyt *b* and membrane-bound cyt *c*-556, as discussed later.

Sequence alignment showed that amino acid residues as well as secondary structures in the cluster-binding subdomain are highly conserved between b_6f and bc_1 Rieske ISPs, while those in large subdomains are highly variable. The conservation of the small subdomains could be explained by a constraint due to a similar interaction mode with *b*-type cyts and hydroquinone-binding sites. In contrast, the large subdomains are thought to have evolved to react properly with various membrane-bound *c*-type cyts, that is, cyt *f* and c_1 in b_6f and bc_1 complexes, respectively, or other electron acceptors in the p-side aqueous

phase. These features support the idea that the Rieske ISPs arose from a common ancestor as a redox center functioning in energy conversion systems The large subdomain would have diverged considerably between cytochrome b_6f and bc_1 complexes, while the cluster-binding subdomain was highly conserved during evolution (Schütz et al., 2000).

The E_m values of Rieske ISP in *C. tepidum* and PetC3 protein in *Synechocystis* sp. PCC 6803 are +160 mV and +135 mV, respectively (Knaff and Malkin, 1976; Veit et al., 2016; Schneider et al., 2002). These values are relatively lower than those of other Rieske ISPs in the cyt bc_1 or b_6f complex (E_m = approximately +300 mV) (Zhang et al., 1996; Link et al., 1992; Schröter et al., 1998). The number of hydrogen bonds formed around the [2Fe–2S] clusters was related to the redox potentials of the Rieske ISPs (Fig. S11). The high-redox-type Rieske ISPs of cyt bc_1 or b_6f complexes from spinach chloroplasts, cyanobacterium *M. laminosus*, bovine heart, and α-proteobacterium *P. denitrificans* have eight hydrogen bonds. In low-redox-type *C. tepidum*, a serine residue was replaced with an alanine residue, resulting in seven hydrogen bonds. In the PetC3 protein, a tyrosine residue was further replaced to phenylalanine one, resulting in only six hydrogen bonds (see Table S1 and Fig. S11). Therefore, the redox potentials of the [2Fe–2S] clusters decreased when the number of hydrogen bonds around them decreased, as previously demonstrated (Schröter et al., 1998; Kolling et al., 2007).

Surface properties. The Rieske ISP soluble domains from b_6f and bc_1 complexes have different surface charges at neutral pH (Fig. 5). The numbers of acidic and basic residues in each soluble domain are summarized along with those in their respective subdomains (Table S2). The values of pI calculated with the ExPASy Compute pI/MW tool for overall structures were also different among species (Gasteiger et al., 2003). The pI values are 7.9 in *C. tepidum*, 5.4 in spinach chloroplast, 6.5 in *M. laminosus*, 7.1 in bovine heart and 4.9 in *P. denitrificans*. However, the cluster-binding subdomains have considerably fewer charged residues than large subdomains and are characterized by nearly equal numbers of acidic and basic residues, thus resulting in almost neutral surface properties. In particular, the peripheral regions just adjacent to surface-exposed clusters are non-polar and are supposed to interact with both the Q_o-site of cyt *b* and the prosthetic group of the electron acceptor, heme *c* or *f*, as discussed in detail later.

In contrast, the differences in acidic and basic residue numbers in large subdomains primarily contribute to all the pIs of the Rieske ISPs. Although the β-barrel-like structures are highly conserved in large subdomains, their surface charges seem to have no relevance to either the interactions of the Rieske ISP soluble domains with their redox partners or the pHs in local areas where they function in the electron transport pathways. In fact, the pI of *C. tepidum* Rieske ISP is a little basic, whereas the other proteins, regardless of whether they are bc_1-or b_6f-type, are weakly acidic or at least neutral (Table S2).

2.4. NMR analysis of the interactions between Rieske$_{sol}$ protein and cyt *c*-556$_{sol}$

Interaction sites on Rieske ISP. Electrons can be transferred efficiently from the Rieske ISP to cyt *c*-556 as previously demonstrated (Oh-oka et al., 1998). To visualize their direct interaction sites, we attempted to crystallize the Rieske$_{sol}$ protein complexed with cyt *c*-556$_{sol}$. Unfortunately, we obtained only crystals of the Rieske$_{sol}$ protein in the mixture drops containing these two proteins. This could be due to weak association properties that allow high turnover numbers by repeating a transient complex formation between them (Iwata et al., 1999). In fact, the pull-down assay using the His-tagged Rieske$_{sol}$ protein attached to the Ni^{2+}-*NTA* resin did not succeed in binding cyt *c*-556$_{sol}$. In these situations, NMR spectroscopy to explore interaction sites between two soluble proteins is a powerful and definitive tool. Chemical shift perturbations can be detected even if these interactions are relatively weak. In addition, the molecular weight of the Rieske$_{sol}$ protein is sufficiently small and suitable for NMR analyses. Therefore, NMR measurements were performed using the uniformly ^{15}N-labeled Rieske$_{sol}$ ([U–^{15}N]-Rieske$_{sol}$) protein as a probe to identify its residue-level interaction sites when it formed a complex with cyt *c*-556$_{sol}$.

We first mixed [U–^{15}N]-Rieske$_{sol}$ protein with cyt *c*-556$_{sol}$. Almost no chemical shift changes were observed. Both proteins were mostly in the oxidized states when their absorption spectra were measured. The findings indicate that their different redox states were necessary for their

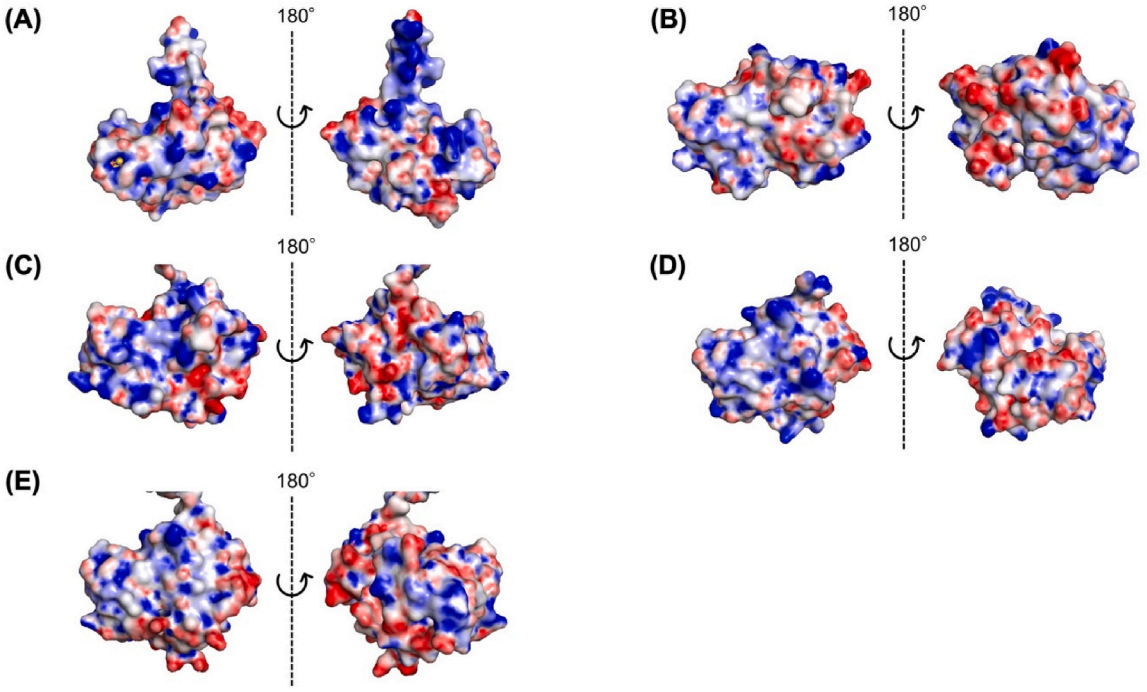

Fig. 5. Electrostatic properties of the surfaces of soluble domains of Rieske ISPs from *C. tepidum* (A), spinach chloroplast (B), cyanobacterium *M. laminosus* (C), bovine heart (D) and α-proteobacterium *P. denitrificans* (E) calculated by PyMOL APBS tool. The distribution is colored according to the electrostatic potential from $-10k_BT$ (red) to $+10k_BT$ (blue). (For interpretation of the references to color in this figure legend, the reader is referred to the Web version of this article.)

interaction to be observed. We then prepared fully reduced [U–^{15}N]-Rieske$_{sol}$ protein and oxidized cyt *c*-556$_{sol}$ by adding a reducing reagent of ascorbate and an oxidizing reagent of ferricyanide, respectively. After mixing, the chemical shift changes due to their interactions could be detected (Fig. S12). Nevertheless, some perturbations were suspected to be derived from direct conformational changes upon the reduction and/or oxidation of the [U–^{15}N]-Rieske$_{sol}$ protein itself, but not upon the specific interaction with cyt *c*-556$_{sol}$. Fortunately, the freshly prepared cyt *c*-556$_{sol}$ was partially reduced (55%), and the cyt *c*-556$_{sol}$ used for the first time in the NMR measurement was fully oxidized during a long-term storage for approximately 2 years at −80 °C (Fig. S13). The redox potentials were reported to be very close to each other, that is, +160 mV for the Rieske ISP and +190 mV for cyt *c*-556 (Knaff and Malkin, 1976). Therefore, when the oxidized [U–^{15}N]-Rieske$_{sol}$ protein and partially reduced cyt *c*-556$_{sol}$ were mixed, their association was expected to proceed and reach redox equilibrium.

Small but discernible changes in the chemical shifts were observed for the peaks from residues located in the belt region around the cluster-binding subdomain comprising Ile123, Leu130, His132, Trp133, Asp134, Ala141, Ile156, Ser157, Leu162, and Lys165 (Fig. 6). These residues were almost the same as those identified in a sample containing chemically reduced [U–^{15}N]-Rieske$_{sol}$ protein and oxidized cyt *c*-556$_{sol}$ (Fig. S12), and thus were considered to be involved in the complex formation between the [U–^{15}N]-Rieske$_{sol}$ protein and cyt *c*-556$_{sol}$ in the electron transfer reaction. However, the shift signals derived from residues on or close to the cluster-binding portion were invisible owing to the paramagnetic effect of Fe(III) of the [2Fe–2S] cluster. The residues responsible for the shift signals were expected to be the most promising direct interaction sites with cyt *c*-556$_{sol}$ from the docking model construction, as described below. We also attempted to prepare Ga-substituted cluster to make it diamagnetic in a similar manner to that reported for plant-type ferredoxin. However, we failed to reconstitute a stable [2Ga-2S] cluster in the Rieske$_{sol}$ protein, probably due to a different combination of ligand residues (two cysteine and two histidine residues) in the Rieske ISP (Mutoh et al., 2015; Kazanis et al., 1995).

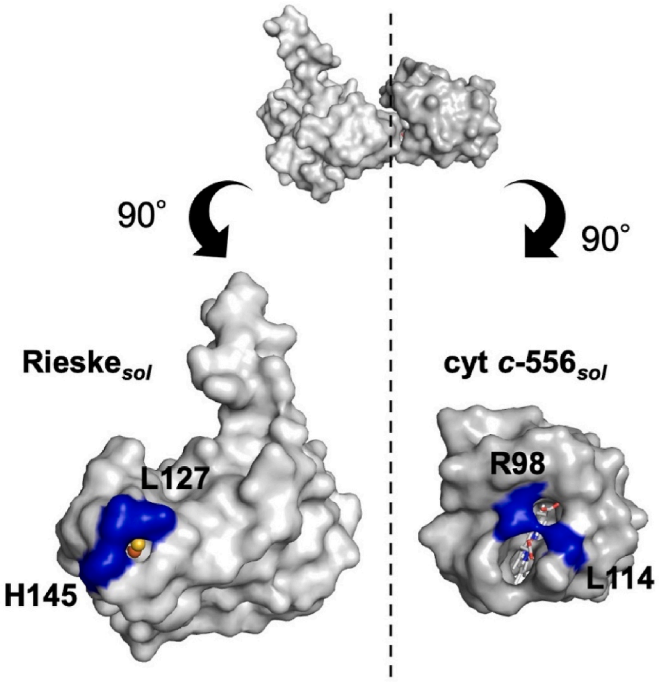

Fig. 7. Open book view of the docking model of Rieske$_{sol}$ protein and cyt *c*-556$_{sol}$. Non-polar interaction formed between them are shown in blue. No electrostatic interactions were observed in this complex model. (For interpretation of the references to color in this figure legend, the reader is referred to the Web version of this article.)

NMR measurements were performed at a higher salt concentration of 300 mM NaCl than 50 mM NaCl. Although slightly increased intensities were observed in the chemical shift changes for the peaks of Ala141, Ile156, Leu162, and Lys165, no significant differences were observed for

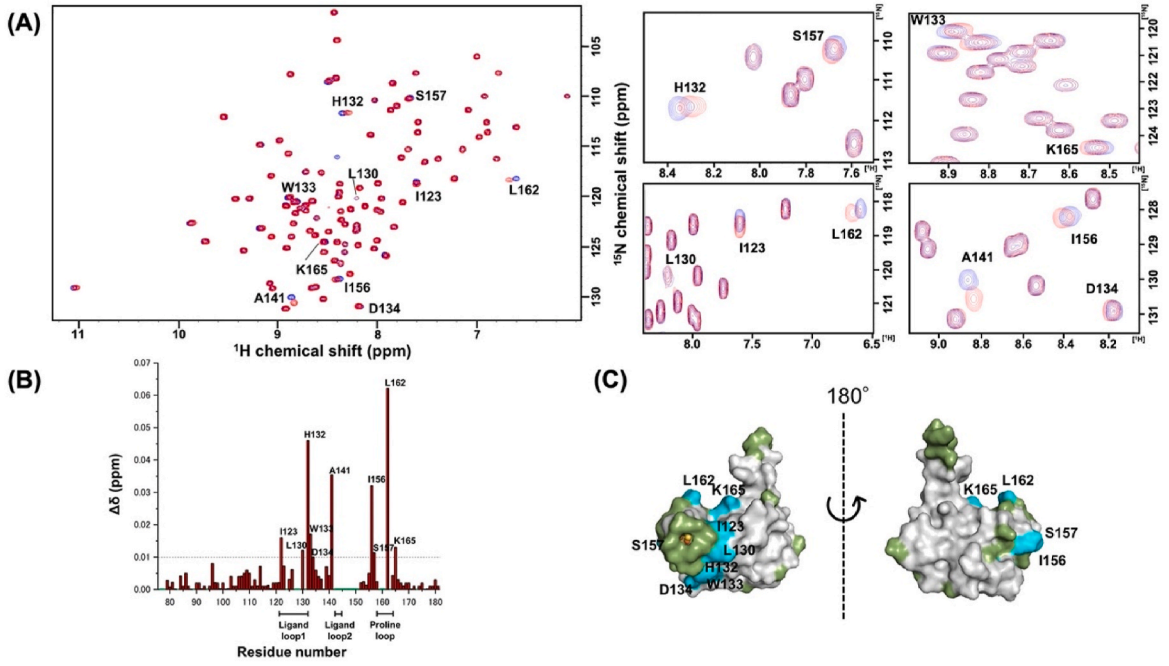

Fig. 6. (A) (Left panel) ^{1}H–^{15}N HSQC spectra of the [U–^{15}N]-Rieske$_{sol}$ protein. Overlay of the HSQC spectra in the absence (shown in blue) and presence (shown in red) of cyt *c*-556. (Right panels) The regions of chemical shifts were enlarged to show slight differences. (B) Chemical shift changes of the [U–^{15}N]-Rieske$_{sol}$ protein after the addition of cyt *c*-556. Residues unable to be assigned are indicated by green lines. (C) Mapping of the chemical shift changes onto the three-dimensional structure of the Rieske$_{sol}$ protein. The residues which were assigned (Δδ>0.01 ppm) and not assigned are colored in cyan and green, respectively. (For interpretation of the references to color in this figure legend, the reader is referred to the Web version of this article.)

the other peaks, indicating that the interaction between the [U–^{15}N]-Rieske$_{sol}$ protein and cyt *c*-556$_{sol}$ was not affected by ionic strength (Fig. S12).

Docking models between Rieske$_{sol}$ protein and cyt c-556$_{sol}$. In addition, a docking model of the Rieske$_{sol}$ protein and cyt *c*-556$_{sol}$ was constructed using the ZDOCK server (Pierce et al., 2014). Protein-protein docking calculations were performed by specifying the amino acid residues of the Rieske$_{sol}$ protein, to which cyt *c*-556$_{sol}$ should be bound based on the above results of NMR chemical shift perturbation experiments of the [U–^{15}N]-Rieske$_{sol}$ protein. Among the ZDOCK outputs, the top ten docking structures ranked based on their ZDOCK scores were examined to determine whether the [2Fe–2S] cluster and heme *c* were faced to each other at closer distances. Three models were adopted as favorable models (Mintseris et al., 2007). The stability of the interaction interface in each model was further assessed in terms of the binding free energy (ΔG_{bind}) estimated by the PDBePISA algorithm in the Protein Data Bank Europe (Krissinel and Henrick, 2007; Krissinel, 2010). The estimates indicated a range of ΔG_{bind} of −9.7 to −5.3 kcal/mol. For the efficient electron transfer, a turnover of association and dissociation between two proteins is important. Thus, their affinity should be adjusted properly to be not too tight or weak. As a reference standard, the ΔG_{bind} between the Rieske ISP and cyt c_1 of bovine cyt bc_1 complex was also estimated as −3.6 kcal/mol, when the closest conformation between them (PDBID: 1BE3) was used from various structures so far determined (Iwata et al., 1998). Finally, we obtained the most probable docking model with $\Delta G_{bind} = -5.3$ kcal/mol (Fig. S14).

The molecular interface of the protein-protein interaction site was checked using Ligplot+ (Laskowski and Swindells, 2011). Hydrogen bond formation was observed between the nitrogen atom (Nε) of H135 of the Rieske$_{sol}$ protein, which is a ligand to an Fe ion (Fe_2) of the [2Fe–2S] cluster, and an oxygen atom (O2D) of the propionate group in heme *c* (Fig. S15A). In the bovine cyt bc_1 complex, a hydrogen bond is formed between the Nε of H161 of the Rieske ISP, which is also a ligand to Fe_2 in the cluster, and O1D of the propionate group in heme *c* (Fig. S15B) (Iwata et al., 1999). Although the two oxygen atoms of the propionate group are indistinguishable in the present heme *c* model, it is nevertheless rational to consider that the model complex of the Rieske$_{sol}$ protein and cyt *c*-556$_{sol}$ exhibits almost the same orientation as the counterpart of the bovine cyt bc_1 complex to enable high turnover rates of electron transfer reactions. Moreover, hydrophobic interactions could also be detected around the cluster and heme pocket of the model complex. As discussed subsequently, the locations seemed to be analogous to those in the bovine cyt bc_1 complex.

3. Discussion

3.1. Transient complex formation by a non-polar interaction

The *in vitro* results of the present NMR measurements revealed that the Rieske$_{sol}$ protein and cyt *c*-556$_{sol}$ could form a weakly associated complex, through which electrons could be transferred between the Rieske [2Fe–2S] cluster and the heme *c*-556 by facing their cofactors with each other (Fig. S14). The prerequisite for this interaction is the redox-state difference between two proteins, which enables the electron transfer reaction to take place between them. The interface of the complex was formed by non-polar or hydrophobic interactions, as indicated by the construction of a docking model (Fig. 7 and S16). No electrostatic attraction from a long-range distance was necessary for both proteins to be close together because the complex was very stable, even under high ionic strength conditions (Fig. S12).

The process of protein-protein interaction and subsequent complex formation in solution can be understood by a two-step model (Ubbink et al., 1998; Volkov et al., 2006). In the model, the formation of the final optimal complex is preceded by the formation of a short-lived, dynamic encounter complex. In the first step, protein association is controlled by long-range electrostatic interactions to make partners close to appropriate orientations. This molecular association step to form an encounter complex consisting of an ensemble of multiple orientations is critical for the formation of a productive and specific conformation that realizes high turnover rates. The final complex with a specific orientation, which is active in electron transfer, is expected to be stabilized by short-range, non-polar interactions, as visualized in the X-ray crystal structure.

Such a stepwise process is a dominant feature of the electron transfer reactions involved in energy conversion systems, such as respiration and photosynthesis, or other metabolic pathways. These pathways have been intensively studied over the past two decades using experimental and theoretical methods, focusing on the transiently formed interfaces. Examples are interfaces between yeast mitochondrial cytochrome *c* peroxidase and cyt *c*, cyt c_1 in the cyt bc_1 complex and cyt *c*, plant/cyanobacterial cyt *f* in the cyt b_6f complex and plastocyanin, and the bacterial RC complex and cyt c_2 (Ubbink et al., 1998; Volkov et al., 2006; Solmaz and Hunte, 2008; Axelrod and Okamura, 2005; Lange and Hunte, 2002). A recent paramagnetic relaxation NMR spectroscopy has shown that the distinction between the encounter and final complexes was ambiguous, and that the encounter complex could also be electron-transfer active any time by increasing non-polar interface areas (Volkov, 2015).

On the other hand, the electron transfer active complex between the Rieske$_{sol}$ protein and cyt *c*-556$_{sol}$ could be formed only by a non-polar interaction, and any charge-related process to the complex formation was precluded, contrary to the interaction process of a two-step model for redox proteins in solution. These two proteins intrinsically function as membrane components that directly transfer electrons to each other without any collisions due to Brownian diffusion. No electrostatic interactions are required for their association. The two proteins are located close each other for easy contact by conformational changes, as discussed below. This interaction mechanism could be interpreted as the reason why we could not obtain a co-crystal of the Rieske$_{sol}$ protein and cyt *c*-556$_{sol}$.

3.2. Functional comparison between cyts c-554 and c-556

The presence of membrane-bound cyt *c*-556 was initially suggested by the discovery of the *c*-type heme showing the α peak wavelength at 556 nm when the chemically reduced-minus-oxidized difference spectrum was measured at a low temperature (77 K) in purified membranes from *C. tepidum* (Oh-oka et al., 1998). Measurements of flash-induced absorption changes also revealed the appearance of a clear shoulder at 556 nm along with a peak at 552 nm, which is responsible for the cyt c_z oxidation, in the presence of stigmatellin, an inhibitor of the Q_o-site of the cyt *bc* complex (Von Jagow and Link, 1986). This was interpreted as evidence of the sequential electron transfer reaction from cyt *c*-556 to cyt c_z after flash excitation; that is, cyt *c*-556 seemed to serve as a cyt c_1-like protein. In contrast, soluble cyt *c*-554 donated electrons directly to cyt c_z in the RC complex in an independent manner from cyt *c*-556 (Tsukatani et al., 2008); cyt *c*-554 did not act like a shuttle-like electron carrier between menaquinol:cytochrome *c* oxidoreductase (cyt *bc* complex) and the P840 RC complex, as seen in the case of cyt c_2 in purple bacteria (Jenney et al., 1994). Cyt *c*-554 was not essential for photosynthetic growth and functioned as an electron carrier from the thiosulfate oxidation pathway to the RC complex (Fig. S1) (Azai et al., 2009).

In this study, the reconstitution experiment showed that cyt *c*-556$_{sol}$ efficiently donated electrons to cyt c_z (Fig. S4). The finding supports the view that the protein encoded by the *CT0073* gene corresponds to the membrane-bound cyt *c*-556. In addition, the NMR measurements provide firm evidence for the direct interaction between cyt *c*-556$_{sol}$ and Rieske$_{sol}$ protein (Fig. 6). Therefore, we conclude that CT0073 is definitely the membrane-bound cyt *c*-556.

The next issue is the factor(s) that discriminate the function between cyts *c-554 and c-556*. The structures of these two proteins are very

similar to each other (Fig. 2D). One barely discernible difference is the relatively hydrophobic nature of the protein surface around the pyrrole ring III edge in cyt *c*-556 compared with the positively charged one in cyt *c*-554 (see Fig. 3 and S6). This region is critical for the association with the Rieske ISP through a non-polar interaction in a limited space area within the membranes, as supported by the results obtained in the present NMR measurements. Another notable difference was the longer loop between the α3 and α4 helices of cyt *c*-554 than that of cyt *c*-556. In the docking model between cyt *c*-556$_{sol}$ and the Rieske$_{sol}$ protein, this loop was identified as the proper site where the protein surface area surrounding the [2Fe–2S] cluster made a direct contact (Fig. S14). In contrast, the longer loop of cyt *c*-554 would prevent the heme from getting close to the cluster, thus hindering complex formation with the Rieske ISP protein (Fig. 8). Positively charged residues on this loop, Lys56 and/or Lys59, are expected to be involved in a long-distance electrostatic interaction with cyt c_z in the RC complex, as suggested by the aforementioned and explained two-step model for the electron transfer mechanism. In fact, the electron transfer rate from cyt *c*-554 to the P840 RC complex reportedly decreases at high salt concentrations (Okumura et al., 1994).

Cyt *c*-556 is supposedly anchored into membranes with the fatty acid chains covalently bound to the thiol group of the N-terminal cysteine residue via a glycerol moiety (Azai et al., 2010). This cytochrome serves as an electron carrier, substituting for cyt c_1/*f* in the typical cyt *bc* complexes. Recent comparative genomic studies have demonstrated that *c*-type cytochrome subunits in cyt *bc* complexes are completely structurally unrelated proteins. Rieske/cyt*b* complexes have thus been proposed to be core proteins, into which various heme proteins are incorporated during the evolution of bioenergetic membranes to flow electrons to the acceptors, coupled with the proton gradient formation (Schütz et al., 2000; Nitschke et al., 2010). Phylogenetic analysis indicated that soluble cyt *c*-554 and membrane-anchored cyt *c*-556 diverged from a common ancestor. This is supported by the close location in the genome of genes encoding their respective CT0075 and CT0073 proteins. The two *c*-type cytochromes would have differentiated functions, as needed during evolution (Tsukatani et al., 2008; Azai et al., 2010).

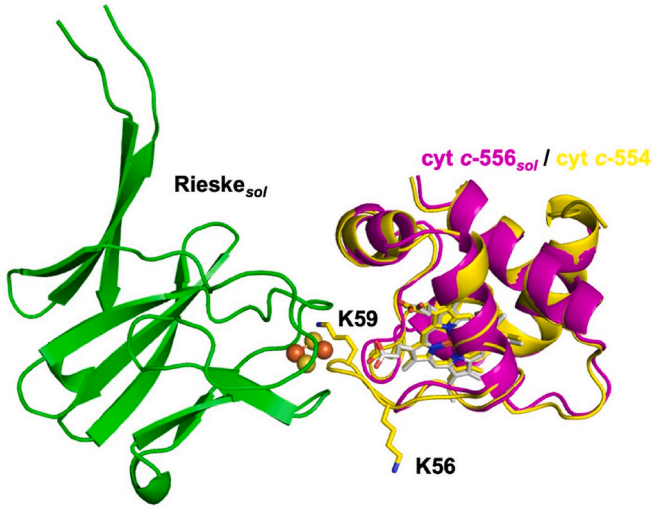

Fig. 8. Docking model of the Rieske$_{sol}$ protein and cyt *c*-556$_{sol}$. The three-dimensional structure of cyt *c*-554 was also superposed to that of cyt *c*-556$_{sol}$ by PyMOL. The longer loop of cyt *c*-554 is indicated to be crushed to the Rieske$_{sol}$ protein, when it locates in the same position of cyt *c*-556 on the electron transfer reaction. This loop contains two lysine residues, Lys 56 and Lys59, which are expected to be involved in a long-distance electrostatic interaction between cyt *c*-554 and cyt c_z.

3.3. Rieske/cytb complex with cyt c-556

As discussed above, menaquinol:cytochrome *c* oxidoreductase in *C. tepidum*, which directly donates electrons to cyt c_z in the RC complex without any soluble carriers, is the Rieske/cyt*b* complex that is tightly associated with membrane-bound cyt *c*-556 (Fig. S17). In 1994, the transcription unit containing *petCB*, which code for Rieske ISP and cyt *b*, was reported to lack the third gene of *petC* for cyt c_1 in *C. limicola*, a species belonging to the green clade, Chlorobiacea (Schütz et al., 1994). Since then, we have been searching for an electron carrier functionally equivalent to cyt c_1 using a combination of biochemical and spectroscopic methods. In the present study, we identified it as cyt *c*-556, encoded by the *CT0073* gene in *C. tepidum* (Figs. S2–S4).

The structure of the Rieske protein in *C. tepidum* has a bilobal shape, similar to that of the chloroplast-type protein (Carrell et al., 1997). However, the reaction partner to which electrons are transferred is not an *f*-type cytochrome usually seen in plant chloroplasts and cyanobacteria. Rather, it is a *c*-type cytochrome in proteobacteria. Therefore, the large subdomain characteristic of the chloroplast-type Rieske proteins is not a critical factor in determining a specific association with *f*-type cytochromes. This domain faces in the opposite direction to both the hemes *b* and *c*, and does not appear to interact with any other components when the three-dimensional structures of cytochrome *bc* complexes are examined (Azai et al., 2010; Kurisu et al., 2003; Kleinschroth et al., 2011).

The exposed domain, or a soluble domain in this study, of the Rieske ISP, which is bound to membranes by a single membrane-spanning α-helix, is mobile between cyts *b* and c_1 (or *f*) during the catalytic cycle of quinol oxidation (Iwata et al., 1998; Di Trani et al., 2022). Because the linker length (five amino acid residues) of the Rieske ISP in *C. tepidum* is relatively shorter by about half compared to those (eight amino acid residues) in chloroplast-type ISP (Fig. S4), the spatial range of its motion might be too small. Nevertheless, two distinct orientations of the Rieske [2Fe–2S] cluster were observed with ESR spectroscopy, strongly indicating exposed domain movements with respect to the membranes (Brugna et al., 1998). The NMR data of the [U–^{15}N]-Rieske$_{sol}$ protein revealed the chemical shift perturbations when mixed with cyt *c*-556$_{sol}$. Unfortunately, direct interaction sites near the [2Fe–2S] cluster could not be observed because of the paramagnetic effect of Fe(III). The protein surface region identified by the present chemical shifts, however, appeared to correspond to the almost equivalent residue sites in the bovine Rieske ISP, which caused significant conformational changes between the c_1-and *Int*-positions, as reported in the X-ray structural analysis of the cyt bc_1 complex (Iwata et al., 1998). These regions would be common in Rieske ISPs, whre interacted with heme cofactors by swinging their heads.

Cyt *b* in *C. tepidum* is not split into two parts, cyt b_6 and subunit IV, although its structural features are very similar to the cyt b_6f-type, for example, the 14 amino acid residues between heme-ligating histidine residues in the fourth transmembrane helix and the lack of the eighth transmembrane helix at the C-terminus. It should be noted that oxidant-induced reduction of cyt *b* was observed in membranes after flash excitation in the presence of antimycin A, which is an inhibitor at the Q_i-site in typical cyt bc_1 complexes (Oh-oka et al., 1998; Tsukatani et al., 2008).

While the exposed domain of the Rieske ISP swings between the Q_o-site of cyt *b* and heme *c* of cyt *c*-556, cyt c_z also fluctuates between cyt *c*-556 and the P840 (Fig. S17). Electrons are thus transferred from the Rieske ISP to the P840 RC only through membrane-associated cyt *c*-556 and cyt c_z. These electron transfer reactions on the surface of the membrane are characterized by swings of the exposed domains. In electron transfer between proteins in very close proximity, hydrophobic and/or non-polar interactions are important for their efficient reaction to be achieved, as revealed in the present study. In green sulfur photosynthetic bacteria, menaquinol:cytochrome *c* oxidoreductase could therefore be defined as cyt *bc* complex.

4. Materials and methods

4.1. Construction of the truncated cyt c-556 expression plasmid

The truncated cyt *c*-556 expression plasmid was constructed as previously described (Higuchi et al., 2009). A fragment from 193 to 429 bp in the *CT0073* gene encoding the C-terminal heme-containing moiety of cyt *c*-556 from Ala65 to Lys143 (designated as the C-cyt *c*-556) was amplified by PCR using the following primer pairs based on the sequence of the *CT0073* gene: (forward) 5′-AAACCATGGCGGAAGGCAAGA CCATTTA-3′ and (reverse) 5′-AAAGGATCCTTATTTCGAGATGCTGAT CAGG-3' (restriction sites are underlined). Primers corresponding to the 5′ ends were designed to introduce a NcoI site in the forward primer and a BamHI site in the reverse primer. The PCR fragment was digested with NcoI/BamHI restriction enzymes (TaKaRa Bio Inc., Shiga, Japan) and inserted into the multiple cloning site of the expression vector pET-20b (+) (Novagen Inc., Madison, WI, USA) which carries an N-terminal pelB signal sequence for the potential periplasmic localization of the target proteins. Cloning results were confirmed by nucleotide sequencing of the entire coding regions.

4.2. Overexpression and purification of the cyt c-556$_{sol}$

For expression of cyt *c*-556$_{sol}$, the plasmid constructed as describe above was co-transformed with pEC86 plasmid (a generous gift from Dr. Linda Thöny-Meyer) into *E. coli* strain C41(DE3) (Arslan et al., 1998; Miroux and Walker, 1996). A 7.5 ml pre-culture was prepared by growing at 37 °C for 7 h in a LB medium supplemented with 100 μg ml^{-1} ampicillin and 33 μg ml^{-1} chloramphenicol. After the inoculation into a 750 ml of LB medium supplemented with the same concentrations of antibiotics, cells were grown at 30 °C for 60 h by gentle stirring at 60–75 rpm using a non-bladed Erlenmeyer flask avoiding foaming. Cells were harvested by centrifugation (10,000×*g*) at 4 °C for 10 min. Iopropyl-1-thio-β-D-galactopyranoside (IPTG) induction step to overexpress the cyt *c*-556$_{sol}$ was not performed. This was because the addition of IPTG caused traffic congestion by over-expressed apo-cyt *c*-556$_{sol}$, which should be exported into the periplasmic space, resulting in its accumulation in the cytosolic space. Cyt *c*-556$_{sol}$ was extracted by osmotic shock following the procedure described in the Novagen pET System Manual (11th Edition). After concentration using the Viospin 6-3K ultrafiltration method (Sartorius AG, Göttingen, Germany), cyt *c*-556$_{sol}$ was purified by size exclusion chromatography using HiLoad 26/600 Superdex 75 pg resin (GE Healthcare, Piscataway, NJ, USA) equilibrated with 50 mM Tris–HCl (pH 8.0) and 150 mM NaCl.

4.3. Crystallization of cyt c-556$_{sol}$

The purified cyt *c*-556$_{sol}$ was concentrated to 30 mg ml^{-1} and crystallized by the hanging-drop vapor-diffusion method at 20 °C. Each drop consisted of 0.5 μl of protein solution and 0.5 μl of precipitant solution equilibrated against 500 μl of precipitant reservoir. Crystals were obtained in 0.1 M sodium acetate trihydrate (pH 4.4) and 1.8 M ammonium sulfate.

4.4. X-ray diffraction experiment and structure determination of cyt c-556$_{sol}$

The cyt *c*-556$_{sol}$ crystals were soaked in a cryoprotectant solution containing 0.1 M sodium acetate (pH 4.6), 2.0 M ammonium sulfate, and 20% glycerol for 10 s and then flash-cooled at 100 K. Diffraction data were collected at 100 K using a synchrotron radiation beam at the SPring-8 BL44XU synchrotron beamline. The complete data set was collected from a single crystal. Diffraction data were processed and scaled using the HKL-2000 software package (Otwinowski and Minor, 1997).

The crystal structure of cyt *c*-556$_{sol}$ was determined by the SAD method using anomalous signals from the heme iron. The structure was refined using the Refmac5 and COOT software (Emsley and Cowtan, 2004; Winn et al., 2011; Murshudov et al., 1997). The final structure included 79 (Ala45-Lys143) residues, excluding the plasmid-derived Met and the original N-terminal moiety of the membrane-anchor domain.

4.5. Construction of the truncated Rieske ISP (PetC) expression plasmid

A fragment from 226 to 543 bp in the *petC* gene encoding the soluble domain of the Rieske ISP from Ala76 to Ala181 was amplified by PCR using the following primer sets: (forward) 5′-AAACATATGGC CAAAAAGATCAAGATCGTC-3′ and (reverse) 5′-AAAAAGCTTCGC-TATCGAAACAACAATCTTA-3′ (restriction site underlined). Primers corresponding to the 5′ ends were designed to introduce an NdeI site in the forward primer and HindIII site in the reverse primer. The PCR product was digested with NdeI/HindIII restriction enzymes (Toyobo Inc., Osaka, Japan), subcloned into pUC118, and the sequence was confirmed. Following digestion of pUC118-*petC*$_{sol}$ with NdeI/HindIII, the DNA fragment containing the *petC*$_{sol}$ gene was ligated into the pET21a(+) vector (Novagen, Madison, WI, USA), and pET21a(+)-*petC*$_{sol}$-His6 was generated.

4.6. Overexpression and purification of the Rieske$_{sol}$ protein

The pET21a(+)-*petC*$_{sol}$-His6 expression vector was transformed into *E. coli* strain C41(DE3) cells harboring the plasmid pRKISC, which contains the *isc* gene cluster involved in the assembly of the Fe–S cluster (Takahashi and Nakamura, 1999). The cells were cultivated at 37 °C in Terrific broth containing 100 μg ml^{-1} ampicillin and 10 μg ml^{-1} tetracycline to an absorbance of approximately 0.3 at 600 nm. The expression of Rieske$_{sol}$ protein in pET21a(+)-*petC*$_{sol}$-His6 vector was induced with 0.1 mM IPTG after supplementation with 0.1 mg ml^{-1} ferric ammonium citrate, and the cells were then grown for 20 h at 25 °C.

The cells were harvested by centrifugation, resuspended in 50 mM Tris–HCl buffer (pH 7.5) containing 10% (w/v) glycerol, 4 mg lysozyme, and 400 mM phenylmethyl sulfonyl fluoride, and disrupted by sonication. After the removal of undisrupted cells and insoluble matters by centrifugation, the supernatant was applied to Ni^{2+}-*NTA* affinity column (QIAGEN, Carlsbad, CA, USA) equilibrated with 50 mM Tris–HCl (pH8.0) and 300 mM NaCl. The C-terminal His-tagged Rieske$_{sol}$ protein was eluted with 50 mM Tris–HCl (pH8.0), 300 mM NaCl, and 250 mM imidazole, and further purified by gel filtration chromatography using HiLoad 26/600 Superdex 75 pg resin (GE Healthcare) equilibrated with 20 mM Tris–HCl (pH7.5) and 50 mM NaCl.

4.7. Overexpression of SeMet-Rieske$_{sol}$ protein

For the Se-SAD analysis, Met139 in Rieske$_{sol}$ protein was substituted with SeMet as previously described (Guerrero et al., 2001; LeMaster and Richards, 1985). Since it was unknown whether *E. coli* strain B834 (DE3) cells can harbor the pRKISC, cells harboring only the pET21a(+)-*petC*$_{sol}$-His6 vector were grown at 37 °C in LeMaster medium containing 50 μg ml^{-1} ampicillin to an absorbance of approximately 0.3 at 600 nm. The expression of SeMet-Rieske$_{sol}$ protein was induced with 0.1 mM IPTG, and the cells were grown for 19 h at 20 °C. SeMet-Rieske$_{sol}$ protein was purified as described above.

4.8. Overexpression of the uniformly ^{13}C, ^{15}N-labeled Rieske$_{sol}$ protein

The pET21a(+)-*petC*$_{sol}$-His6 vector was transformed into in *E. coli* strain C41(DE3) cells harboring the plasmid pRKISC. The [U–^{15}N] and [U–^{13}C,^{15}N] labeled Rieske$_{sol}$ proteins were overexpressed in M9 minimum medium containing 1.0 g L^{-1} $^{15}NH_4Cl$ in the absence or presence of 4.0 g L^{-1} [U–^{13}C]-D-glucose (Cambridge Isotope Laboratories, Inc., Tewksbury, MA, USA). The cells were cultivated at 37 °C to an

absorbance of approximately 0.3 at 600 nm. The expression of the labeled Rieske$_{sol}$ protein was induced with 0.1 mM IPTG, the cells were grown for 20 h at 25 °C, and labeled Rieske$_{sol}$ protein was purified as described above.

4.9. Crystallization of Rieske$_{sol}$ protein

The purified Rieske$_{sol}$ protein was concentrated to 45 mg ml^{-1} with ultrafiltration of Vivaspin 5 k (Sartorius). Crystallization was performed using the hanging-drop vapor-diffusion method at 293K, with each drop consisting of 1 μl of protein solution and 1 μl of the reservoir solution.

Initial trials were performed using the commercially available sparse-matrix screening kits Crystal Screens I and II (Hampton Research, Aliso Viejo, CA, USA) and Wizards I and II (Emerald Biostructures, Bainbridge Island, WA, USA). The initial conditions that produced crystals were optimized by varying the concentrations of protein, precipitants, buffer systems, and pH. The crystallization conditions finally established consisted of a protein solution of 10 mg ml^{-1} in 20 mM Tris–HCl (pH 7.5), containing 50 mM NaCl, and a reservoir solution consisting of 0.2M ammonium sulfate, 0.1 M ammonium citrate (pH5.0), and 22% (w/v) polyethylene glycol 2,000. Although the X-ray diffraction data of the crystals were collected, their initial phases were not determined using the molecular replacement method. Therefore, we aimed to solve this structure using the SAD technique with selenium as the anomalous scattering atom. The SeMet-Rieske$_{sol}$ protein was crystallized under conditions that were slightly different from those used for Rieske$_{sol}$ protein. Crystals were grown in drops containing a 1:1 mixture of protein (50 mg ml^{-1} in 20 mM Tris–HCl (pH 7.5) containing 50 mM NaCl) and a reservoir solution (0.2M ammonium sulfate, 0.1M ammonium citrate (pH5.0), 22% (w/v) polyethylene glycol 2,000, and 10%(v/v) ethanol). The crystals were soaked in a cryoprotectant solution containing 0.2M ammonium sulfate, 0.1M ammonium citrate (pH5.0), 22% (w/v) polyethylene glycol 2,000, and 20% (v/v) ethanol for 10 s and then flash-cooled at 100 K.

4.10. X-ray diffraction experiment and structure determination of Rieske$_{sol}$ protein

Diffraction data were collected at 100 K using the SPring-8 BL44XU synchrotron radiation beam source. The complete data set was collected from a single crystal. Diffraction data were processed and scaled using the HKL-2000 software package (Otwinowski and Minor, 1997).

The crystal structure of the Rieske$_{sol}$ protein was determined by the SAD method using anomalous signals from the selenium iron in Se-labeled methionine. The structure was refined using the Refmac5 and COOT software (Emsley and Cowtan, 2004; Winn et al., 2011; Murshudov et al., 1997). The final structure was 110 residues long (Lys77-Ala186), including a part of the C-terminal His-tag (Lys182-Ala186).

4.11. NMR measurement and docking models

NMR experiments were conducted on an Avance III HD 600 spectrometer using QCI-P cryogenic probes with an ^{1}H resonance frequency of 600 MHz (Bruker, Billerica, MA, USA). Sequence-specific assignments were made from the two-dimensional ^{1}H–^{15}N heteronuclear single-quantum coherence (HSQC) and three-dimensional HNCA, HN(CO)CA, HNCO, HN(CA)CO, HNCACB, and CBCA(CO)NH spectra of 1.36 mM [U–^{13}C, ^{15}N]-Rieske$_{sol}$ protein dissolved in 20 mM Tris–HCl buffer (pH 7.5) containing 50 mM NaCl at 298 K. Spectrum data was analyzed by NMRFAM-Sparky and I-PINE web server (Lee et al., 2015, 2019). The gene for the Rieske$_{sol}$ protein encodes 114 amino acids including 6 Pro residues.

The 80 ^{1}H–^{15}N peaks were assigned to the ^{1}H–^{15}N HSQC spectrum of the Rieske$_{sol}$ protein (Fig. S18). The peaks of amino acid residues I79-G88, A90-V93, N95–I123, T125-I140, A147, K148, I155–S157, L164-E172, and G174-A181 were detected. A76-K78, P89, P94, C124, A141-G146, Y149–K154, G158-P163 and D173 were not detected. In particular, peaks of residues in loop 2 could not be detected because of paramagnetic iron atoms of the [2Fe–2S] cluster.

Chemical shift perturbation experiments were performed by recording two-dimensional ^{1}H–^{15}N HSQC spectra of 100 μM [U–^{15}N]-Rieske$_{sol}$ protein dissolved in 20 mM Tris–HCl buffer (pH 7.5) containing 50 mM NaCl in the absence and presence of 300 μM of cyt *c*-556$_{sol}$ at 298 K. The spectra were measured with ^{1}H and ^{15}N acquisition periods of 106.5 and 45.7 ms, respectively. The experimental time for each spectrum was 1 h with 16 scans accumulated for each free induction decay. The redox states of both the proteins were confirmed by measuring their absorption spectra using a model UV-3101PC spectrophotometer (Shimadzu, Kyoto, Japan).

All NMR data were processed using TopSpin (Bruker) and the spectra were analyzed using NMRFAM-Sparky (Guerrero et al., 2001). The weighted averages of ^{1}H and ^{15}N chemical shift changes were calculated using the formula $\Delta\delta = [(\Delta\delta^{1}_{HN})^{2} + (0.04\Delta\delta^{15}_{N})^{2}]^{1/2}$ (Mutoh et al., 2015). The simulated docking models were calculated using ZDOCK by submitting the coordinates to the ZDOCK Web server (Pierce et al., 2014). The binding free energy for each protein complex model was estimated using the PDBePISA on the Protein Data Bank Europe website (Krissinel and Henrick, 2007; Krissinel, 2010). Protein-protein interactions were further examined using Ligplot+ (Laskowski and Swindells, 2011).

Accession number

Assigned resonances for Rieske$_{sol}$ protein was deposited in the BMRB with accession number 51723. The coordinate and structure factor of Rieske$_{sol}$ protein and cyt *c*-556$_{sol}$ was deposited in Protein Data Bank under accession number 8HN2 and 8HN3, respectively.

CRediT authorship contribution statement

Hiraku Kishimoto: Protein expression and characterization, Crystallization, NMR measurement, Formal analysis, Protein-protein docking model, Visualization, Writing – original draft, Writing – review & editing. **Chihiro Azai:** Conceptualization, Protein characterization, Formal analysis, Writing – review & editing. **Tomoya Yamamoto:** Protein expression and characterization, Crystallization, Formal analysis. **Risa Mutoh:** Crystallization, Formal analysis, Writing – review & editing. **Tetsuko Nakaniwa:** Crystallization, Formal analysis. **Hideaki Tanaka:** Conceptualization, 3D structure analysis, Validation, Writing – review & editing. **Yohei Miyanoiri:** Conceptualization, NMR analysis, Supervision, Validation, Writing – review & editing. **Genji Kurisu:** Conceptualization, 3D structure analysis, Supervision, Validation, Writing – review & editing. **Hirozo Oh-oka:** Conceptualization, Protein characterization, Project administration, Supervision, Validation, Writing – original draft, Writing – review & editing.

Declaration of competing interest

The authors declare the following financial interests/personal relationships which may be considered as potential competing interests: Hirozo Oh-oka reports financial support was provided by Japan Society for the Promotion of Science. Chihiro Azai reports financial support was provided by Japan Society for the Promotion of Science. Risa Mutoh reports financial support was provided by Japan Society for the Promotion of Science. Genji Kurisu reports financial support was provided by JST-CREST.

Data availability

Data will be made available on request.

Acknowledgements

This work was supported by Grants-in-Aid for Scientific Research (Nos. 21K06220, 21H05266, 22H02030 to C. A., No. 15K21122 to R.M., and Nos. T18K061530 and T21K061120 to H.O.), JST-CREST (JPMJCR20E1 to G.K.), and JSPS Grants-in-Aid for Scientific Research on Innovative Areas (No. 19H04724 to H.O.) from MEXT.

Appendix A. Supplementary data

Supplementary data to this article can be found online at https://doi.org/10.1016/j.crstbi.2023.100101.

References

Ambler, R.P., 1991. Sequence variability in bacterial cytochromes *c*. Biochim. Biophys. Acta 1058, 42–47.

Arslan, E., Schulz, H., Zufferey, R., Künzler, P., Thöny-Meyer, L., 1998. Overproduction of the *Bradyrhizobium japonicum c*-type cytochrome subunits of the cbb_3 oxidase in *Escherichia coli*. Biochem. Biophys. Res. Commun. 251, 744–747.

Axelrod, H.L., Okamura, M.Y., 2005. The structure and function of the cytochrome c_2: reaction center electron transfer complex from *Rhodobacter sphaeroides*. Photosynth. Res. 85, 101–114.

Azai, C., Tsukatani, Y., Harada, J., Oh-oka, H., 2009. Sulfur oxidation in mutants of the photosynthetic green sulfur bacterium *Chlorobium tepidum* devoid of cytochrome *c*-554 and SoxB. Photosynth. Res. 100, 57–65.

Azai, C., Tsukatani, Y., Itoh, S., Oh-oka, H., 2010. *C*-type cytochromes in the photosynthetic electron transfer pathways in green sulfur bacteria and heliobacteria. Photosynth. Res. 104, 189–199.

Baker, N.A., Sept, D., Joseph, S., Holst, M.J., McCammon, J.A., 2001. Electrostatics of nanosystems: application to microtubules and the ribosome. Proc. Natl. Acad. Sci. U. S. A 98, 10037–10041.

Baymann, F., Lebrun, E., Nitschke, W., 2004. Mitochondrial cytochrome c_1 is a collapsed di-heme cytochrome. Proc. Natl. Acad. Sci. U. S. A 101, 17737–17740.

Bersch, B., Blackledge, M.J., Meyer, T.E., Marion, D., 1996. *Ectothiorhodospira halophila* ferrocytochrome c_{551}: solution structure and comparison with bacterial cytochromes *c*. J. Mol. Biol. 264, 567–584.

Bönisch, H., Schmidt, C.L., Schäfer, G., Ladenstein, R., 2002. The structure of the soluble domain of an archaeal Rieske iron-sulfur protein at 1.1 Å resolution. J. Mol. Biol. 319, 791–805.

Brugna, M., Albouy, D., Nitschke, W., 1998. Diversity of Cytochrome *bc* Complexes: example of the Rieske protein in green sulfur bacteria. J. Bacteriol. 180, 3719–3723.

Cape, J.L., Bowman, M.K., Kramer, D.M., 2006. Understanding the cytochrome *bc* complexes by what they don't do. The Q-cycle at 30. Trends Plant Sci. 11, 46–55.

Carrell, C.J., Zhang, H.M., Cramer, W.A., Smith, J.L., 1997. Biological identity and diversity in photosynthesis and respiration: structure of the lumen-side domain of the chloroplast Rieske protein. Structure 5, 1613–1625.

Carter, D.C., Melis, K.A., O'Donnell, S.E., Burgess, B.K., Furey, W.F., Wang, B.C., Stout, C. D., 1985. Crystal structure of *Azotobacter* cytochrome c_5 at 2.5 Å resolution. J. Mol. Biol. 184, 279–295.

Davidson, E., Daldal, F., 1987. Primary structure of the bc_1 complex of *Rhodopseudomonas capsulata*: nucleotide sequence of the *pet* operon encoding the rieske cytochrome *b*, and cytochrome c_1 apoproteins. J. Mol. Biol. 195, 13–24.

Di Trani, J.M., Liu, Z.L., Whitesell, L., Brzezinski, P., Cowen, L.E., Rubinstein, J.L., 2022. Rieske head domain dynamics and indazole-derivative inhibition of *Candida albicans* complex III. Structure 30, 129–138.

Dolinsky, T.J., Nielsen, J.E., McCammon, J.A., Baker, N.A., 2004. PDB2PQR: an automated pipeline for the setup of Poisson-Boltzmann electrostatics calculations. Nucleic Acids Res. 32, W665–W667.

Emsley, P., Cowtan, K., 2004. *Coot*: model-building tools for molecular graphics. Acta Crystallographica Section D-Structural Biology 60, 2126–2132.

Gasteiger, E., Gattiker, A., Hoogland, C., Ivanyi, I., Appel, R.D., Bairoch, A., 2003. ExPASy: the proteomics server for in-depth protein knowledge and analysis. Nucleic Acids Res. 31, 3784–3788.

Guerrero, S.A., Hecht, H.J., Hofmann, B., Biebl, H., Singh, M., 2001. Production of selenomethionine-labelled proteins using simplified culture conditions and generally applicable host/vector systems. Appl. Microbiol. Biotechnol. 56, 718–723.

Hauska, G., Schoedl, T., Remigy, H., Tsiotis, G., 2001. The reaction center of green sulfur bacteria. Biochim. Biophys. Acta Bioenerg. 1507, 260–277.

Higuchi, M., Hirano, Y., Kimura, Y., Oh-oka, H., Miki, K., Wang, Z.Y., 2009. Overexpression, characterization, and crystallization of the functional domain of cytochrome c_z from *Chlorobium tepidum*. Photosynth. Res. 102, 77–84.

Hirano, Y., Higuchi, M., Azai, C., Oh-oka, H., Miki, K., Wang, Z.Y., 2010. Crystal structure of the electron carrier domain of the reaction center cytochrome c_z subunit from green photosynthetic bacterium *Chlorobium tepidum*. J. Mol. Biol. 397, 1175–1187.

Holm, L., 2022. Dali server: structural unification of protein families. Nucleic Acids Res. 50. W210-W5.

Itoh, M., Seo, D., Sakurai, H., Sétif, P., 2002. Kinetics of electron transfer between soluble cytochrome *c*-554 and purified reaction center complex from the green sulfur bacterium *Chlorobium tepidum*. Photosynth. Res. 71, 125–135.

Iwata, S., Saynovits, M., Link, T.A., Michel, H., 1996. Structure of a water soluble fragment of the 'Rieske' iron sulfur protein of the bovine heart mitochondrial cytochrome bc_1 complex determined by MAD phasing at 1.5 Å resolution. Structure 4, 567–579.

Iwata, S., Lee, J.W., Okada, K., Lee, J.K., Iwata, M., Rasmussen, B., Link, T.A., Ramaswamy, S., Jap, B.K., 1998. Complete structure of the 11-subunit bovine mitochondrial cytochrome bc_1 complex. Science 281, 64–71.

Iwata, M., Björkman, J., Iwata, S., 1999. Conformational change of the Rieske [2Fe-2S] protein in cytochrome bc_1 complex. J. Bioenerg. Biomembr. 31, 169–175.

Jenney, F.E., Prince, R.C., Daldal, F., 1994. Roles of the soluble cytochrome c_2 and membrane-associated cytochrome c_y of *Rhodobacter capsulatus* in photosynthetic electron transfer. Biochemistry 33, 2496–2502.

Kabsch, W., Sander, C., 1983. Dictionary of protein secondary structure: pattern recognition of hydrogen-bonded and geometrical features. Biopolymers 22, 2577–2637.

Kazanis, S., Pochapsky, T.C., Barnhart, T.M., Pennerhahn, J.E., Mirza, U.A., Chait, B.T., 1995. Conversion of a FE_2S_2 ferredoxin into a Ga^{3+} rubredoxin. J. Am. Chem. Soc. 117, 6625–6626.

Kjær, B., Scheller, H.V., 1996. An isolated reaction center complex from the green sulfur bacterium *Chlorobium vibrioforme* can photoreduce ferredoxin at high rates. Photosynth. Res. 47, 33–39.

Kleinschroth, T., Castellani, M., Trinh, C.H., Morgner, N., Brutschy, B., Ludwig, B., Hunte, C., 2011. X-ray structure of the dimeric cytochrome bc_1 complex from the soil bacterium *Paracoccus denitrificans* at 2.7-Å resolution. Biochim. Biophys. Acta Bioenerg. 1807, 1606–1615.

Knaff, D.B., Malkin, R., 1976. Iron-sulfur proteins of green photosynthetic bacterium *chlorobium*. Biochim. Biophys. Acta 430, 244–252.

Kolling, D.J., Brunzelle, J.S., Lhee, S., Crofts, A.R., Nair, S.K., 2007. Atomic resolution structures of Rieske iron-sulfur protein: role of hydrogen bonds in tuning the redox potential of iron-sulfur clusters. Structure 15, 29–38.

Kramer, D.M., Cruz, J.A., Kanazawa, A., 2003. Balancing the central roles of the thylakoid proton gradient. Trends Plant Sci. 8, 27–32.

Krissinel, E., 2010. Crystal contacts as nature's docking solutions. J. Comput. Chem. 31, 133–143.

Krissinel, E., Henrick, K., 2007. Inference of macromolecular assemblies from crystalline state. J. Mol. Biol. 372, 774–797.

Kurisu, G., Zhang, H.M., Smith, J.L., Cramer, W.A., 2003. Structure of the cytochrome b_6f complex of oxygenic photosynthesis: tuning the cavity. Science 302, 1009–1014.

Lange, C., Hunte, C., 2002. Crystal structure of the yeast cytochrome bc_1 complex with its bound substrate cytochrome *c*. Proc. Natl. Acad. Sci. U. S. A 99, 2800–2805.

Laskowski, R.A., Swindells, M.B., 2011. LigPlot+: multiple ligand-protein interaction diagrams for drug discovery. J. Chem. Inf. Model. 51, 2778–2786.

Lee, W., Tonelli, M., Markley, J.L., 2015. NMRFAM-SPARKY: enhanced software for biomolecular NMR spectroscopy. Bioinformatics 31, 1325–1327.

Lee, W., Bahrami, A., Dashti, H.T., Eghbalnia, H.R., Tonelli, M., Westler, W.M., Markley, J.L., 2019. I-PINE web server: an integrative probabilistic NMR assignment system for proteins. J. Biomol. NMR 73, 213–222.

LeMaster, D.M., Richards, F.M., 1985. ^1H-^{15}N heteronuclear NMR studies of *Escherichia coli* thioredoxin in samples isotopically labeled by residue type. Biochemistry 24, 7263–7268.

Liebschner, D., Afonine, P.V., Baker, M.L., Bunkóczi, G., Chen, V.B., Croll, T.I., Hintze, B., Hung, L.W., Jain, S., McCoy, A.J., Moriarty, N.W., Oeffner, R.D., Poon, B.K., Prisant, M.G., Read, R.J., Richardson, J.S., Richardson, D.C., Sammito, M.D., Sobolev, O.V., Stockwell, D.H., Terwilliger, T.C., Urzhumtsev, A.G., Videau, L.L., Williams, C.J., Adams, P.D., 2019. Macromolecular structure determination using X-rays, neutrons and electrons: recent developments in *Phenix*. Acta Crystallographica Section D Structural Biology 75, 861–877.

Link, T.A., Hagen, W.R., Pierik, A.J., Assmann, C., Von Jagow, G., 1992. Determination of the redox properties of the Rieske [2Fe-2S] cluster of bovine heart bc_1 complex by direct electrochemistry of a water-soluble fragment. Eur. J. Biochem. 208, 685–691.

Majumder, E.L.W., Blankenship, R.E., 2016. The diversity of photosynthetic cytochromes. Cytochrome Complexes: Evolution, Structures, Energy Transduction, and Signaling 41, 25–50.

Mendz, G.L., Smith, M.A., Finel, M., Korolik, V., 2000. Characteristics of the aerobic respiratory chains of the microaerophiles *Campylobacter jejuni* and *Helicobacter pylori*. Arch. Microbiol. 174, 1–10.

Mintseris, J., Pierce, B., Wiehe, K., Anderson, R., Chen, R., Weng, Z.P., 2007. Integrating statistical pair potentials into protein complex prediction. Proteins: Struct., Funct., Bioinf. 69, 511–520.

Miroux, B., Walker, J.E., 1996. Over-production of proteins in *Escherichia coli*: mutant hosts that allow synthesis of some membrane proteins and globular proteins at high levels. J. Mol. Biol. 260, 289–298.

Murshudov, G.N., Vagin, A.A., Dodson, E.J., 1997. Refinement of macromolecular structures by the maximum-likelihood method. Acta Crystallographica Section D-Structural Biology 53, 240–255.

Mutoh, R., Muraki, N., Shinmura, K., Kubota-Kawai, H., Lee, Y.H., Nowaczyk, M.M., Rögner, M., Hase, T., Ikegami, T., Kurisu, G., 2015. X-Ray structure and nuclear magnetic resonance analysis of the interaction sites of the Ga-substituted cyanobacterial ferredoxin. Biochemistry 54, 6052–6061.

Nagashima, H., Kishimoto, H., Mutoh, R., Terashima, N., Oh-Oka, H., Kurisu, G., Mino, H., 2017. Hyperfine sublevel correlation spectroscopy studies of iron-sulfur cluster in rieske protein from green sulfur bacterium *Chlorobaculum tepidum*. J. Phys. Chem. B 121, 2543–2553.

Nitschke, W., Van Lis, R., Schoepp-Cothenet, B., Baymann, F., 2010. The "green" phylogenetic clade of Rieske/cyt*b* complexes. Photosynth. Res. 104, 347–355.

Oh-oka, H., Kamei, S., Matsubara, H., Iwaki, M., Itoh, S., 1995. 2 molecules of cytochrome *c* function as the electron donors to P840 in the reaction center complex isolated from a green sulfur bacterium. Chlorobium tepidum. Febs Letters 365, 30–34.

Oh-oka, H., Iwaki, M., Itoh, S., 1998. Membrane-bound cytochrome c_z couples quinol oxidoreductase to the P840 reaction center complex in isolated membranes of the green sulfur bacterium *Chlorobium tepidum*. Biochemistry 37, 12293–12300.

Okumura, N., Shimada, K., Matsuura, K., 1994. Photooxidation of membrane-bound and soluble cytochrome *c* in the green sulfur bacterium *Chlorobium tepidum*. Photosynth. Res. 41, 125–134.

Otwinowski, Z., Minor, W., 1997. Processing of X-ray diffraction data collected in oscillation mode. Macromolecular Crystallography, Pt A. 276, 307–326.

Pierce, B.G., Wiehe, K., Hwang, H., Kim, B.H., Vreven, T., Weng, Z.P., 2014. ZDOCK server: interactive docking prediction of protein-protein complexes and symmetric multimers. Bioinformatics 30, 1771–1773.

Schneider, D., Skrzypczak, S., Anemüller, S., Schmidt, C.L., Seidler, A., Rögner, M., 2002. Heterogeneous Rieske proteins in the cytochrome b_6f complex of *Synechocystis* PCC6803? J. Biol. Chem. 277, 10949–10954.

Schröter, T., Hatzfeld, O.M., Gemeinhardt, S., Korn, M., Friedrich, T., Ludwig, B., Link, T. A., 1998. Mutational analysis of residues forming hydrogen bonds in the Rieske [2Fe-2S] cluster of the cytochrome bc_1 complex in Paracoccus denitrificans. Eur. J. Biochem. 255, 100–106.

Schütz, M., Zirngibl, S., Lecoutre, J., Büttner, M., Xie, D.L., Nelson, N., Deutzmann, R., Hauska, G., 1994. A transcription unit for the Rieske FeS-protein and cytochrome *b* in *Chlorobium limicola*. Photosynth. Res. 39, 163–174.

Schütz, M., Brugna, M., Lebrun, E., Baymann, F., Huber, R., Stetter, K.O., Hauska, G., Toci, R., Lemesle-Meunier, D., Tron, P., Schmidt, C., Nitschke, W., 2000. Early evolution of cytochrome *bc* complexes. J. Mol. Biol. 300, 663–675.

Solmaz, S.R.N., Hunte, C., 2008. Structure of complex III with bound cytochrome *c* in reduced state and definition of a minimal core interface for electron transfer. J. Biol. Chem. 283, 17542–17549.

Sommer, F., Drepper, F., Haehnel, W., Hippler, M., 2006. Identification of precise electrostatic recognition sites between cytochrome c_6 and the photosystem I subunit PsaF using mass spectrometry. J. Biol. Chem. 281, 35097–35103.

Sone, N., Tsuchiya, N., Inoue, M., Noguchi, S., 1996. Bacillus stearothermophilus *qcr* operon encoding Rieske FeS protein, cytochrome b_6, and a novel-type cytochrome c_1 of quinol-cytochrome *c* reductase. J. Biol. Chem. 271, 12457–12462.

Takahashi, Y., Nakamura, M., 1999. Functional assignment of the ORF2-*iscS-iscU-iscA-hscB-hscA-fdx*-ORF3 gene cluster involved in the assembly of Fe-S clusters in *Escherichia coli*. J. Biochem. 126, 917–926.

Terwilliger, T.C., Adams, P.D., Read, R.J., McCoy, A.J., Moriarty, N.W., Grosse-Kunstleve, R.W., Afonine, P.V., Zwart, P.H., Hung, L.W., 2009. Decision-making in structure solution using Bayesian estimates of map quality: the *PHENIX AutoSol* wizard. Acta Crystallogr. Sect. D Biol. Crystallogr. 65, 582–601.

Tetreault, M., Cusanovich, M., Meyer, T., Axelrod, H., Okamura, M.Y., 2002. Double mutant studies identify electrostatic interactions that are important for docking cytochrome c_2 onto the bacterial reaction center. Biochemistry 41, 5807–5815.

Tsukatani, Y., Azai, C., Kondo, T., Itoh, S., Oh-oka, H., 2008. Parallel electron donation pathways to cytochrome c_z in the type I homodimeric photosynthetic reaction center complex of *Chlorobium tepidum*. Biochim. Biophys. Acta Bioenerg. 1777, 1211–1217.

Ubbink, M., Ejdebäck, M., Karlsson, B.G., Bendall, D.S., 1998. The structure of the complex of plastocyanin and cytochrome *f*, determined by paramagnetic NMR and restrained rigid-body molecular dynamics. Structure 6, 323–335.

Veit, S., Takeda, K., Tsunoyama, Y., Baymann, F., Nevo, R., Reich, Z., Rögner, M., Miki, K., 2016. Structural and functional characterisation of the cyanobacterial PetC3 Rieske protein family. Biochim. Biophys. Acta Bioenerg. 1857, 1879–1891.

Volkov, A.N., 2015. Structure and function of transient encounters of redox proteins. Acc. Chem. Res. 48, 3036-2043.

Volkov, A.N., Worrall, J.A.R., Holtzmann, E., Ubbink, M., 2006. Solution structure and dynamics of the complex between cytochrome *c* and cytochrome c peroxidase determined by paramagnetic NMR. Proc. Natl. Acad. Sci. U. S. A 103, 18945–18950.

Von Jagow, G., Link, T.A., 1986. Use of specific inhibitors on the mitochondrial bc_1 complex. Methods Enzymol. 126, 253–271.

Winn, M.D., Ballard, C.C., Cowtan, K.D., Dodson, E.J., Emsley, P., Evans, P.R., Keegan, R. M., Krissinel, E.B., Leslie, A.G.W., McCoy, A., McNicholas, S.J., Murshudov, G.N., Pannu, N.S., Potterton, E.A., Powell, H.R., Read, R.J., Vagin, A., Wilson, K.S., 2011. Overview of the *CCP4* suite and current developments. Acta Crystallographica Section D-Structural Biology 67, 235–242.

Worrall, J.A.R., Schlarb-Ridley, B.G., Reda, T., Marcaida, M.J., Moorlen, R.J., Wastl, J., Hirst, J., Bendall, D.S., Luisi, B.F., Howe, C.J., 2007. Modulation of heme redox potential in the cytochrome c_6 family. J. Am. Chem. Soc. 129, 9468–9475.

Yu, L.J., Unno, M., Kimura, Y., Yanagimoto, K., Oh-oka, H., Wang-Otomo, Z.Y., 2013. Structure analysis and characterization of the cytochrome *c*-554 from thermophilic green sulfur photosynthetic bacterium *Chlorobaculum tepidum*. Photosynth. Res. 118, 249–258.

Zhang, H., Carrell, C.J., Huang, D.R., Sled, V., Ohnishi, T., Smith, J.L., Cramer, W.A., 1996. Characterization and crystallization of the lumen side domain of the chloroplast Rieske iron-sulfur protein. J. Biol. Chem. 271, 31360–31366.